



Article

Towards Manufacturing of Ultrafine-Laminated Structures in Metallic Tubes by Accumulative Extrusion Bonding

Matthew R. Standley and Marko Knezevic *

Department of Mechanical Engineering, University of New Hampshire, Durham, NH 03824, USA; mrx46@wildcats.unh.edu

* Correspondence: marko.knezevic@unh.edu

Abstract: A severe plastic deformation process, termed accumulative extrusion bonding (AEB), is conceived to steady-state bond metals in the form of multilayered tubes. It is shown that AEB can facilitate bonding of metals in their solid-state, like the process of accumulative roll bonding (ARB). The AEB steps involve iterative extrusion, cutting, expanding, restacking, and annealing. As the process is iterated, the laminated structure layer thicknesses decrease within the tube wall, while the tube wall thickness and outer diameter remain constant. Multilayered bimetallic tubes with approximately 2 mm wall thickness and 25.25 mm outer diameter of copper-aluminum are produced at 52% radial strain per extrusion pass to contain eight layers. Furthermore, tubes of copper-copper are produced at 52% and 68% strain to contain two layers. The amount of bonding at the metal-to-metal interfaces and grain structure are measured using optical microscopy. After detailed examination, only the copper-copper bimetal deformed to 68% strain is found bonded. The yield strength of the copper-copper tube extruded at 68% improves from 83 MPa to 481 MPa; a 480% increase. Surface preparation, as described by the thin film theory, and the amount of deformation imposed per extrusion pass are identified and discussed as key contributors to enact successful metal-to-metal bonding at the interface. Unlike in ARB, bonding in AEB does not occur at ~50% strain revealing the significant role of more complex geometry of tubes relative to sheets in solid-state bonding.

Keywords: plasticity; strength; metallic tubes; finite element analysis; accumulative extrusion bonding



Citation: Standley, M.R.; Knezevic, M. Towards Manufacturing of Ultrafine-Laminated Structures in Metallic Tubes by Accumulative Extrusion Bonding. *Metals* 2021, *11*, 389. https://doi.org/10.3390/met11030389

Academic Editors: Andrew Kennedy, Gabriel Centeno Báez and Maria Beatriz Silva

Received: 15 January 2021 Accepted: 23 February 2021 Published: 27 February 2021

Publisher's Note: MDPI stays neutral with regard to jurisdictional claims in published maps and institutional affiliations.



Copyright: © 2021 by the authors. Licensee MDPI, Basel, Switzerland. This article is an open access article distributed under the terms and conditions of the Creative Commons Attribution (CC BY) license (https://creativecommons.org/licenses/by/4.0/).

1. Introduction

Bimetallic materials have been used for components delivering different material properties by their geometry (e.g., inside versus outside of a tube) [1–4]. Such components achieve benefits, such as lower cost for the consumer and producer, reduced weight, simplification of design, and/or reduced number of parts in a structure or assembly [3]. Bimetallic materials could be manufactured in the form of tubular geometries to serve desired applications. When employing bimetallic tubes, for example, one material can provide strength and stability, while the other can offer better corrosion resistance. A two-layer copper-steel tube, for example, can handle high loads via the steel and the corrosion resistance via the copper [4].

Bonding between the bimetals is not always necessary, and ultimately depends on the application. The two-layer designs typically rely on each material to perform one aspect of the intended design function independent of the other. In this case, a very tight compression fit between the two constituent metals may be appropriate. Evolving from the two-layer concept, multilayered material is envisioned for even more demanding or unique applications. To this end, multilayered materials provide a blended, and most often optimized, set of material properties but require each layer to be bonded to the next to do so.

Multilayered bimetallic manufacturing is a relatively new frontier in manufacturing and delivers superior material characteristics when compared to the constituent materials.

Metals **2021**, 11, 389 2 of 25

Many material combinations have been reported as bonded using accumulative roll bonding (ARB) such as Cu/Ti [5], Al/Cu [6], Al/Zn [7], Mg/Al [8], Cu/Zn/Al [9], Cu/Zn [10], Zr/Nb [11,12], Mg/Nb [13,14] and Zn/Sn [15] in plate form. When the layering is pushed to the ultrafine micron, or ultimately nanometer scale, the multilayered bimetallic material exhibits significantly improved strength [16–24], thermal stability [25,26], resistance to shock damage [27], and resistance to radiation damage [28,29]. Beyond this, the authors of [30] summarize the history of laminated metal composites and other benefits of bimetallic materials, such as improved fracture resistance, delayed fatigue crack growth, and ballistic energy absorption.

This work explores a processing methodology for manufacturing multilayered bimetallic tubing to achieve similar improvements in material properties to ARB sheets. To the knowledge of the authors at the time of publication, no research has reported producing multilayered bimetallic tubing using any severe plastic deformation processes. Following previous research in extrusion to achieve bimetallic tubing [31], this work takes inspiration from their design to develop a more complete manufacturing process. The process is termed accumulative extrusion bonding (AEB) and is used, in an iterative sense, to create single metal and bimetallic tubing with several layers. AEB, like ARB, is a severe plastic deformation process, which is defined as a metal forming process that creates very high strain without significant change to the overall dimensions to produce substantial grain refinement using severe straining and high levels of hydrostatic pressure [11,32–39]. By doing so, a decrease in grain size can improve the material properties following the Hall-Petch relationship [40–42] and increase the material strength by a factor of three to eight [43]. Additionally, as reported in [44], materials with ultrafine grains can have good damping properties, exhibit lower temperature super-plasticity, and high magnetic properties.

The AEB process involves iterative extrusion, cutting, expanding, restacking, and annealing. Due to the increased complexity of maintaining the geometrical shape of tubing relative to sheets, AEB is a much more challenging process than ARB. Other severe plastic deformations processes exist to produce extruded tube, and are well documented in the following review article [45]. Such processes include Equal Channel Angular Pressing (ECAP), Tube Channel Pressing (TCP), Tubular Channel Angular Pressing (TCAP), among others [45–47]. Since restacking and reprocessing is essential in producing ultrafine grains in multilayered tubing, AEB is described herein.

When this AEB process is compared to other AEB processes, the main differences include geometry of the extruded material, the custom dies and setup used, and the expansion process. Additionally, AEB performed in [48] did not use intermittent annealing, and because of this, tracked the true strain increase as samples were continuously processed. The AEB process used in the present research, utilizes annealing after every severe plastic deformation step such that accounting for continuous strain is not needed as strain effects are removed. Additionally, no material specimen or die preheat is used as indicated in the research performed in [49]. Most unique, no research has reported using AEB to manufacture multilayered bimetals in the form of tube as current research utilizes plate or sheet as done in [48–51]. For this reason, as part of the AEB process used for this research, expansion is necessary to facilitate restacking.

Two sets of specialty tooling are designed for a hydraulic press: One imparting 52% radial strain and another imparting 68% radial strain to produce the tubing. The design process is aided by finite element (FE) simulations to better understand the mechanics of the severe plastic deformation operations. After making the tooling, several similar and dissimilar metallic tubes are created to evaluate the extent of bonding, microstructure, and material properties. Hardness of the materials, yield strength, and ultimate tensile strength are compared before and after processing. Moreover, grain structure and the amount of bonding at the metal-to-metal interfaces are measured using optical microscopy. Surface preparation and the amount of deformation imposed per extrusion pass are discussed as critical to successful metal-to-metal bonding at the interface. Future work will attempt to create ultrafine multilayered bimetallic tubes with micron to nano radial lay-

Metals 2021, 11, 389

amount of bonding at the metal-to-metal interfaces are measured using optical microscopy. Surface preparation and the amount of deformation imposed per extrusion pass are discussed as critical to successful metal-to-metal bonding at the interface. Future work will attempt to create ultrafine multilayered bimetallic tubes with micron to nano radial layers of alternating material with many metal-metal interfaces governing a unique set of material properties.

2. Methods

2. Methods 2.1. Theory of Bonding 2.1. Theory of Bonding

The thin film theory prevails as the primary explanation for bimetal bonding in high The thin film theory prevails as the primary explanation for bimetal bonding in high pressure cold rolling. Like rolling, extrusion is also a high-pressure process in which the pressure cold rolling. Like rolling, extrusion is also a high-pressure process in which the theory is viable as other mechanisms that explain bonding are unlikely to occur. Other theory is viable as other mechanisms that explain bonding are unlikely to occur. Other such bonding mechanisms are diffusion, overcoming energy barrier, and joint recrystallization 1521. A brief summary of the theory is as follows:

1. Avery thin brittle surface must exist on both metallic faces to be bonded.

2. Under high pressure, the metallic faces are forced into one interface where the thin brittle surfaces on both metallale sies to cook and an asignificant unto timpo and strain.

3. Through the mallitracks from hir rain in a material is truthen which interact with the ore position in the interact of the position and the interact of the position in the interact of the

In ARB applications, the brittle surfaces are prepared by light scratch brushing using stainless brushes, and the high pressure is provided by rolls. For example, nickel plated Cu/A153bp/Ma/g/Janid 31/241/Ai/Ni41/5andaAd/Al/Sal shertshwere were were using using using this niguni inthi invois, wish prasuroris survidest by actico a mandral mandar pumbunyon tech in ally distributed terminal participation are are expressed as the contraction of the co unFlgInetagn biagendicatadibatkerbutklennublearantersynnered anben arbender under prossives to the other hinch shows hourd) auriditial initigating aposentrebene and administration of the constraint of t interthintellies. This is unfurtely ast dears at examination still engine of conformation and parel pareed usual built at haith bribblist beus far a cevis stiss. Sa that constant all side overedd into the extrussion ledge im stage 2, the air gapissignificantly reduced, the metall to metall interface is from ed, amd plastic strainoccurs within ithe metasta Du Dtoethe highlstghirs texis is level & scracks within which tiln in the rittle surittees, unfades, in and minimum and the content and extracted the surittees, unfades, in and in the content and extracted the surittees and the surittees and the surittees are the surittees are the surittees and the surittees are the su ordekse in auch bepade Abstachn Eisterien gestage de tearthel executive comprosies a byggers y ibligant the dinagle tithesfineal slespredashagucadeoluterdioanteetdiaaneternaintainaedtainmed idiaeneternoeternoeta metva tueloe table. Some carea many may bondo and another intercome prepare Further persons eightly be preating in the theorems and in the first of a will be continued to the interfaces the first of the interfaces are the inter such that voids, and trappedioxides will be drinned and albed action to emerally literature wherethein helluente on conterial debasion is on is imized [28].

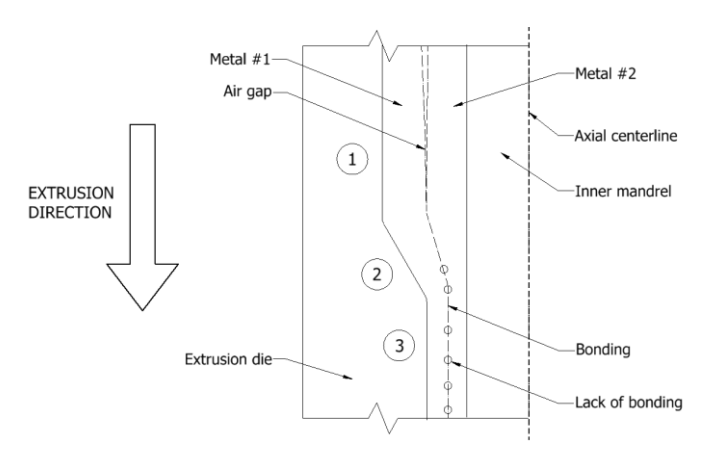
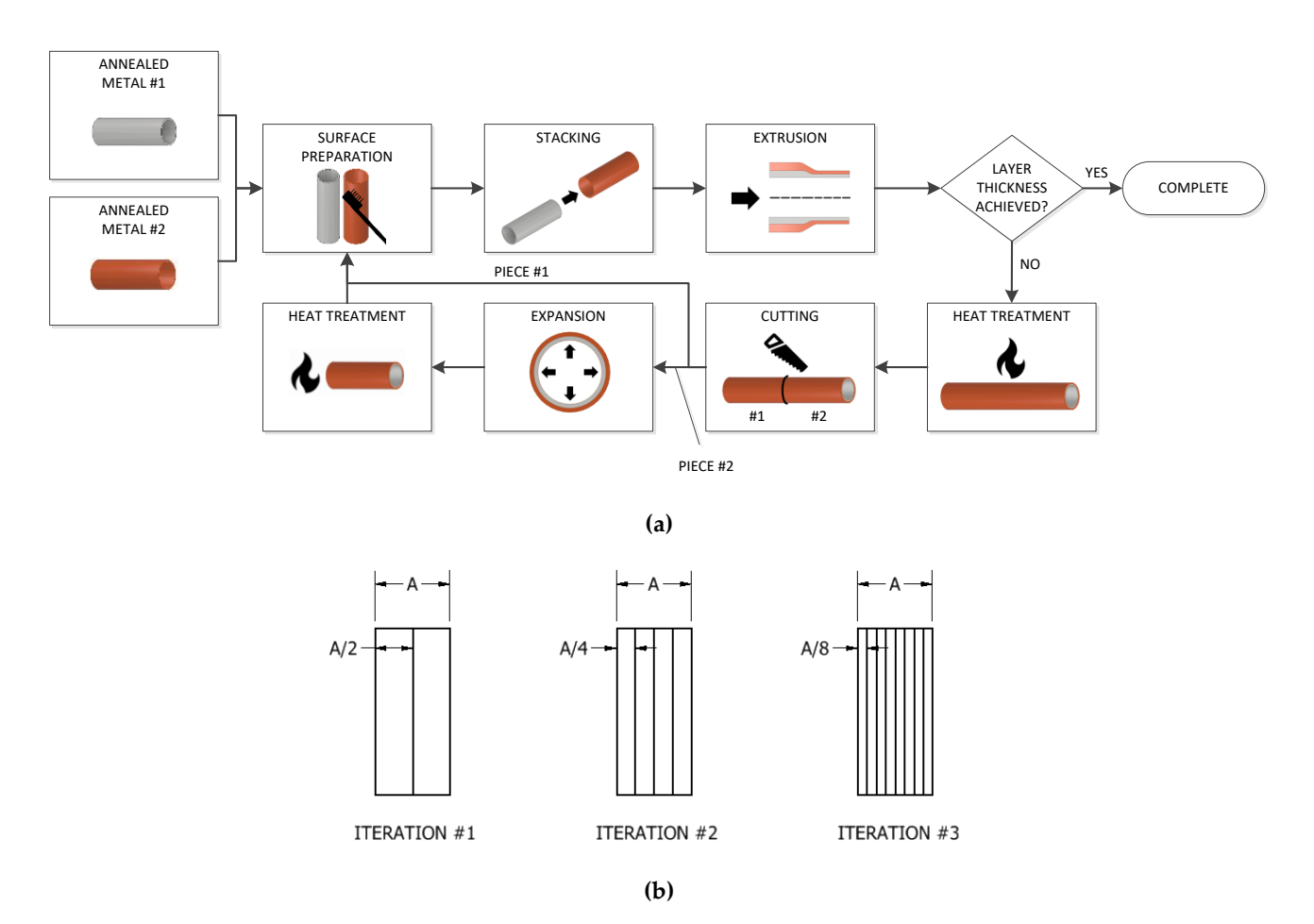


Figure 1. Axis-symmetric cross section of extrusion process and the three stages of bonding using AEB. The metal initially experiences compression (stage 1) before entering the extrusion zone (stage 2), where severe plastic deformation occurs, and exits in the final desired shape (stage 3).



Figlioure(2)(The manufacturing process flow map for achieving without inelaminated structures imendial tube is wAEAEB.

(b) (b) Aphicial education of the comminutation of the co

2.2.1. Surface Preparation

2.2. Manufacturing operation is the simple action of inserting one metal tube into the other.

Before addioperatival tilaperatoristical in titality grip is teas to pad provinte studences, which ive provides a tomobilar microsteristical studences and intelligence. As the Rip the circuit attached a the alay type hilly masses within the their interaction and intelligences and intelligences to the transfer of the studence of the

The Thirt the surface eschieb will she far experience of uninearly uninear will table to the wind of the surface of the surfac

and 19 the distilled water per y layer thickness is the atmosphere for all min After of the acid was neutralized with cool distilled water. The copper was then degreased in an other iteration as shown in Figure 2. The first step to prepare the extruded tube for reprocessing is annealing to restore ductility and bisection at the imidpoint to create two tubes of approximately half the extruded length. One of the two metal tubes is then expanded such that it can fit over its extruded diameter. After another annealing of the expanded tube, the initial process is repeated. This continues until the desired layer

Metals **2021**, 11, 389 5 of 25

thickness is achieved. The exponential decrease in layer thickness, occurring at 2^{i} , is critical in achieving very thin layer thicknesses in a reasonable way.

The two annealing steps, and the initial annealing, are critical to processing and are tactically used to restore ductility before all severe plastic deformation process steps. Based on testing performed, herein, the process flow shown in Figure 2 is the minimum process flow required. Bimetallic tubes produced when omitting any of the annealing steps, for example, caused blistering and tearing during extrusion or expansion.

2.2.1. Surface Preparation

The stacking operation is the simple action of inserting one metal tube into the other. Before this operation is performed, it is critically important to prepare the surfaces, which will become the metal-to-metal interface. In ARB, the interfacial surfaces are typically degreased using acetone and then scratch-brushed with stainless steel bristles [13,53–55]. This surface preparation is reportedly one of the most important steps to achieve full bonding, since it removes the naturally occurring oxide layer and hardens the surface simultaneously. The scratch brushing creates a slightly hardened and brittle outer surface in comparison to the bulk material, due to local strain hardening occurring at the surface. The brittle surface, which will be prone to cracking during extrusion, will allow virgin sub-surface metal to pass through the cracks to contact the virgin material of the other metal to enact bonding. Scratch brushing is applied transverse to the extrusion direction to help promote crack opening.

Before stacking and scratch brushing, acid cleaning is performed to remove any surface impurities. The copper was cleaned by pickling using a solution of 10% sulfuric acid and 90% distilled water per volume. This was done at room temperature for 10 min. After, the acid was neutralized with cool distilled water. The copper was then degreased in an ultrasonic acetone bath for 30 min, where the acetone was drained and replenished halfway through the cleaning process. The aluminum only received degreasing using the ultrasonic acetone bath. After degreasing in acetone, the metal tubes were scratch-brushed and stacked together.

To achieve the most optimal hardened surface, tubes were scratched with stainless steel bristles. The outer diametrical interface was scratched with a handheld stainless-steel brush, while the inner diametrical interface was brushed with a rotary stainless-steel brush. The stainless-steel bristles were 25.4 mm long on the handheld brush with a diameter of 0.305 mm. The stainless-steel bristles on the rotary brush were 13.97 mm long with a diameter of 0.152 mm and rotated at a constant RPM during application. The two different methods of applications were employed due to the curved geometry of each surface.

The surface roughness was measured before and after brushing and is tabulated in Table 1. Surface roughness increased 29.6% and 46.8% respectively on the inner, and outer surfaces, respectively. To find the average surface finish, measurements were taken in 10 random locations on each surface using a Pocket Surf III profilometer (Mahr Federal Inc., Providence, RI, USA). All surface finish values reported before and after brushing are representative of cold extruded aluminum using lubricant for context [57].

Table 1. Average surface roughness before and after scratch brushing.

Process	Surface	Material	Before µm RA√	After μm RA√	% Increase
Rotary brush	Inner diameter	Copper	1.15	1.49	29.6
Handheld brush	Outer diameter	Aluminum	0.32	0.47	46.8

The intent of the brushing is not to induce visible asperities and significantly increase the surface roughness, but to clean the surface of oxidation while hardening it at the same time. Oxidation layer minimization is necessary to aid in bonding, but significantly over-brushing did not improve the amount of bonding. Not quantified by the authors, but reported in literature [52], minimizing the build-up of oxidation is critical to aid in bonding

Metals **2021**, 11, 389 6 of 25

and to reduce additional foreign material inclusion. Beyond scratch brushing, minimizing contact with the atmosphere was employed to discourage further oxidation growth.

After scratch brushing the metal tubes are not cleaned of any debris caused by brushing. Instead, the tubes were lightly tapped to remove any loose particles. Immediately following the acetone cleaning and brushing, the tubes were stacked and extruded. On average, this was performed within 2 min to prevent the naturally occurring oxide layer to fully reform. After 15 min of exposure to air, as reported in another study [58] regarding aluminum bonding, the natural oxide layers begin to markedly interfere with the bonding process.

The scratch brushing method does not produce any noticeable debris from the stainless steel bristles which helped promote cleanliness. Other methods beyond scratch brushing were attempted but were ultimately not used. Metal files, Scotch-BriteTM pads (3M Company, Saint Paul, MA, USA), and various sanding papers were also used with no success. The major issue with these methods is cleanliness control and the lack of versatility to be applied to curved surfaces of the inner and outer diameters. These methods created a lot of non-metallic debris during application and caused too much inconvenience during processing.

2.2.2. Extrusion

The extrusion process bonds the two metals together through severe plastic deformation as described by the thin film theory. Previous research in die geometry has determined an outer ring die paired with a straight mandrel produces the least peak stresses within the die and can successfully achieve enough plastic strain to promote bonding [31]. Therefore, the die angle and geometry are adopted for this research. Figures of the die are presented in the next section. The extrusion process is performed in a 4-pronged die set which was customized to support a self-aligning die and punch. The die, punch, and mandrel are used to maintain the tubular shape and are described in more detail in the die design section. The extrusion was performed at room temperature (approximately 20.5 °C) with an extrusion speed of 2.73 mm/s. No heat was added during extrusion to promote bonding.

The die, mandrel, and punch are coated with a thin layer of extrusion oil to reduce friction and discourage material adhesion. Non-diluted Drawsol[®] WM 4740 (Houghton International, Manchester, England) was used for its ability to maintain high film strength when under extreme pressure. This oil is also recommended for various metals including steel, stainless-steel, titanium, and aluminized alloys. From a processing perspective, this synthetic lubricant is water soluble, which is easily removed with running tap water.

Bimetals are extruded at 52% and 68% deformation which represent how much the outer diameter is reduced during extrusion. These values represent the minimum (50%) [5–9] and mid-range of reported deformation employed in previous research, which achieved bonding using ARB. These deformation values also promote stacking as well; at 52% deformation a 2-layer tube can be re-stacked, and the original die can be reused, while at 68% deformation, 3-layer tube stacking can be utilized. This was done intentionally to reduce the number of required dies. In both cases, the deformation percentage values are slightly more than 1/2 and 2/3 as to provide clearances from the nominal stacking fraction to assist in processing.

2.2.3. Cutting

The second step in the iterative loop, if the bimetallic layer thickness is not achieved, is cutting. Simply, the bimetal is cut to remove the non-bonded section at the end of the bimetallic extrusion, the non-bonded initial section at the start, and then equally in half perpendicular to the extrusion direction. By performing cutting the total material volume is not conserved. Therefore, it is necessary to quantify the expected losses per iteration to ensure a viable end-product is produced. Cutting is performed using a material specimen preparation sawmill using a diamond infused metallurgical cutting disc. After, all edges were deburred with 320 grit sandpaper.

Metals **2021**, 11, 389 7 of 25

2.2.4. Expansion

One of the two extruded tubes require diametrical expansion to facilitate stacking. The chosen tube is expanded such that the inner diameter is increased to a size that is slightly larger than the outer diameter of the extruded tube. This is performed by pushing the tube over a diametrical expansion mandrel. The expansion mandrel utilizes a cylindrical section that tapers at 10° to an enlarged diameter. The punch, which pushed the bimetal into the extrusion die, is the same punch used to push the tube over the expansion ledge. The bimetal is passed over the expansion post multiple times to fully remove spring-back and achieve a cylindrical tube for stacking. The expansion mandrel is described in more detail in the die design section. Other options to expand the tube were considered such as metal spinning as described in [59,60]. Ultimately, it is more desirable to expand the tube using a mandrel because the process is simple, easy to control, and contained to the same experimental setup (i.e., the hydraulic press and die set).

The expansion step does not promote or impact bonding at the interface since bonding occurred during extrusion where significantly large strains (compared to strains experienced during expansion) are imposed. Additionally, from a conservation of volume perspective, the wall thickness of the expanded tube will decrease depending on the amount of deformation imposed (~11% and ~8% for the 52%, and 68% deformation cases, respectively), which will impact layer thickness consistency. Even though wall thicknesses become slightly inconsistent as iterations continue, the intent is to create many interfacing layers, i.e., the ultrafine structures independent on local layer thicknesses. The local deformation conditions also cause non-uniformity in layer thickness.

2.2.5. Heat treatment

During the extrusion and expansion processes, the metal experiences severe plastic deformation, which is causing significant strain hardening. To aid in processing, it is necessary to restore ductility. Additionally, research in ARB, which is similar to AEB, requires intermediate annealing [61]. Initial annealing of the as-received material is performed to remove initial tempers of T6 for aluminum and H58 for copper. The as-received copper is annealed to 426 °C with a 1 h soak time and cooled at a rate of 426 °C/h. The as-received aluminum is annealed to 413 °C with a 2.5 h soak time and cooled at a rate of 28 °C/h. The initial annealing was selected to enhance ductility [62].

Intermediate annealing is performed after every iteration, and the same annealing as described above for annealing aluminum was employed on the bimetal copper-aluminum tubes produced. It was found that annealing was necessary in every iteration step. Multilayered bimetals were attempted with the annealing step omitted, and severe blistering and tearing occurred throughout the tubular wall.

3. Die and Expansion Designs

The experimental setup of the extrusion process is shown in Figure 3a. The setup is installed in a hydraulic press capable of 260 kN (Greenerd Press and Machine Co., Nashua, NH, USA). The press is omitted from figures. As indicated previously, extrusion was performed at 52% and 68% radial strain. The only difference between the two extrusions is the size of the extrusion ledge (i.e. the dimension L, as shown later) to increase the strain from 52% to 68%. The off-the-shelf die set is customized to perform both the extrusion and expansion processes. The extrusion die and the expanding post are easily swapped to either perform the extrusion or expansion process. A cut-away view of the extrusion setup is provided in Figure 3b,c. Critical dimensions are shown in Figure 3c and are tabulated in Table 2.

was performed at 52% and 68% radial strain. The only difference between the two extrusions is the size of the extrusion ledge (i.e. the dimension L, as shown later) to increase the strain from 52% to 68%. The off-the-shelf die set is customized to perform both the extrusion and expansion processes. The extrusion die and the expanding post are easily swapped to either perform the extrusion or expansion process. A cut-away view of the 8 of 25 extrusion setup is provided in Figure 3b,c. Critical dimensions are shown in Figure 3c and are tabulated in Table 2.

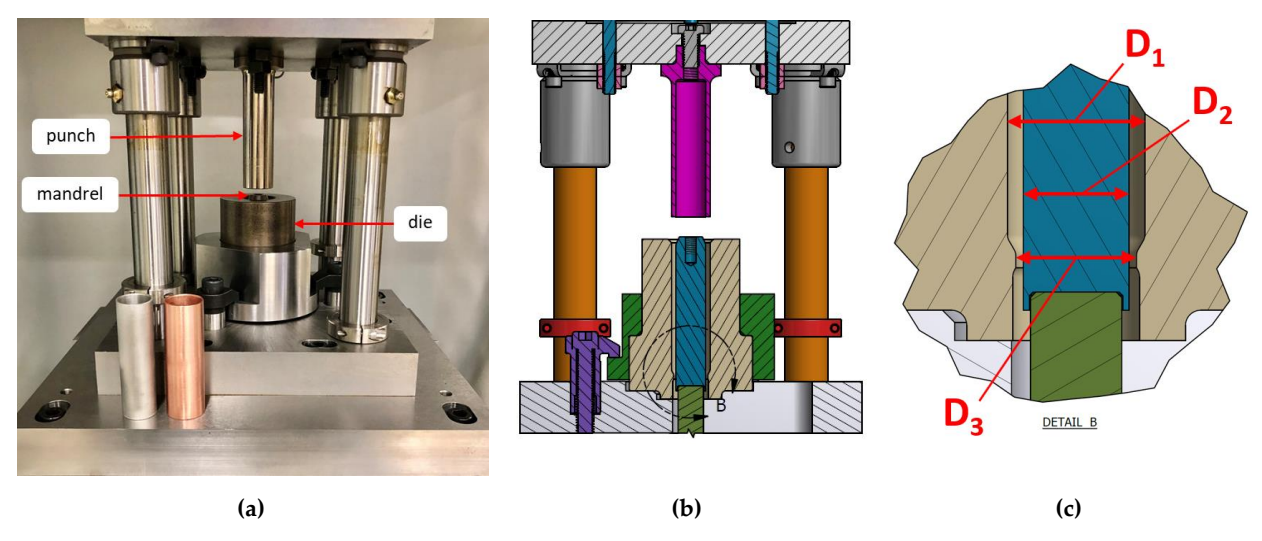


Figure Experimental setup of expression process which provides \$2% which at sin Amount technical hybrautic press. Also depicted is annealed copper and aluminum test metals ready for extrusion. For size perspective, the test metals are also depicted is annealed copper and aluminum test metals ready for extrusion. For size perspective, the test metals are 89 mm in height. This setup is identical to the process which enacts 68% radial strain except for dimension L. (b) Section 89 mm in height. This setup is identical to the process which enacts 68% radial strain except for dimension L. (b) Section view of extrusion setup. (c) Die cavity and extrusion ledge. The tubular bimetal is omitted.

Table 2. Critical dimensional values of extrusion die.

Table	22. Critical dimension Deformation	onal values of extrusion die.	D ₂	D ₃
		mm	mm	mm _
	Deformation 68%	28.70 28.70	22.07 ² 22.0 m	25.25 D ₃ 24.18 mm
	00 /0		22.07	24.10
	52%	28.70	22.07	25.25
	68%	28.70	22.07	24.18

For either the extrusion or the expansion process, both configurations utilize the punch as the mechanism to enact deformation. This was tactically chosen to keep the setup contained to one die set installed in one hydraulic press. Both the die and the expansion post use a floating alignment method. To ensure the punch is always axially aligned neither the extrusion die, nor the expansion post are fixed in place; rather, they both self-align to the punch during setup.

The die is of sufficient length to fully encapsulate the length of the bimetal tubes. This is to ensure it is forced into the extrusion ledge. The extrusion edge geometry, which has a 30° transfer from the initial diameter to the extrusion diameter, has rounded and smooth radii. Just below the extrusion ledge is a diametrical relief for ease of tube removal after the tube is extruded into and past the extrusion ledge. The inner mandrel floats collinear to the die and remains collinear when the bimetal tubes are installed inside the die. The floating mandrel is positioned such that only the least amount of the mandrel is below the extrusion ledge to aid in the removal of the bonded bimetal tube. After extrusion is performed, due to the setup in a hydraulic press, the bimetal tube is removed by removing the die and floating mandrel. For this reason, the floating mandrel is not attached to the vertical support below it. A relief is cut into the bottom portion of the die set, the width slightly larger than an extruded tube, to assist in bimetallic tube removal. Lastly, the punch is designed to insert into the die and have the floating mandrel insert in it. Clearances between these components are less than 2.54×10^{-2} mm.

The expansion post for the expansion process, shown in Figure 4, has a smooth transitional ledge, at 10°, used to expand the bimetal tube such that it can fit over a tube of its original extruded size. A few variations of the expanding post can be used in which the expansion diameter is increased in predetermined increments to aid in processing. Incorporating these variations allows a step-up approach to achieving the final desired inner diameter of an expanded bimetal, if needed. Alternatively, the diameter may be increased directly in one expansion step. For the testing performed, all tubes were directly

ances between these components are less than 2.54×10^{-2} mm.

The expansion post for the expansion process, shown in Figure 4, has a smooth to sitional ledge, at 10°, used to expand the bimetal tube such that it can fit over a tube of original extruded size. A few variations of the expanding post can be used in which expansion diameter is increased in predetermined increments to aid in processing. In porating these variations allows a step-up approach to achieving the final desired in diameter of an expanded bimetal, if needed. Alternatively, the diameter may be increed expanded indirectly the diameter may be increed expanded indirectly the diameter may be increed which can be used sixthing at the later of t

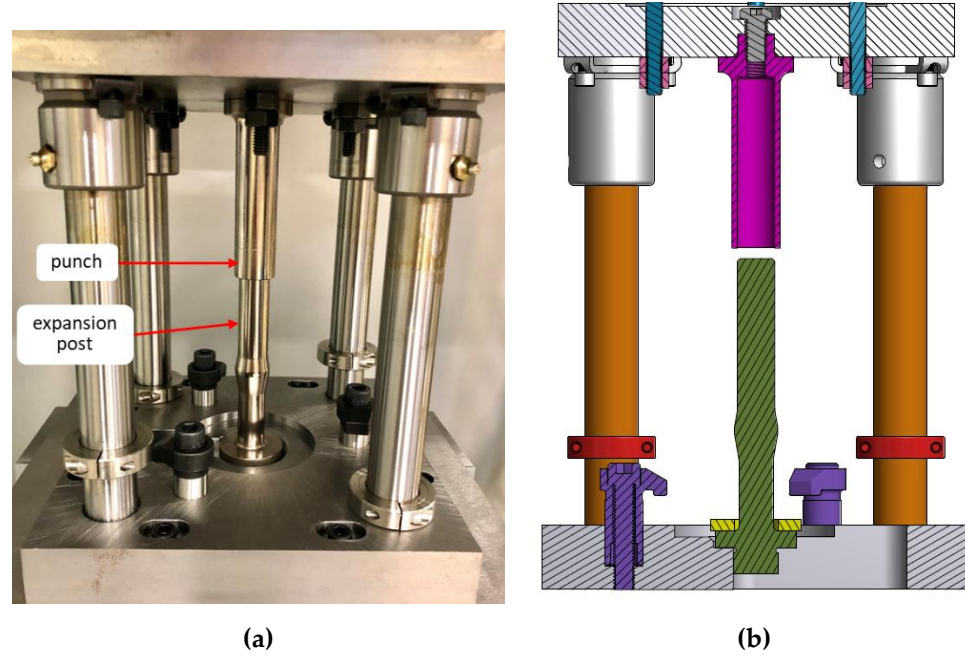


Figure 4. (a) Experimental experimental experimental expension setup. Expansion setup. Expa

The die, pundhendiad punched expansion postexpathsion aposture of the main functional components of the performithen the performing the extremitation of the material for These attended from the second of the third stress material forming processes. The hardness range for these components is 58 to 62 HRC which is a typical range for extrusion and forming dies. The A2 material has desirable characteristics which are tabulated in Table 3. The wear resistance and toughness are improved with the coating described below.

Table 3. Cold work tool steel relative ratings (A = greatest to E = least) [63].

Characteristic	AISI A2 Tool Steel	
Safety in hardening	A	
Depth of hardening	A	
Resistance to decarburization	В	
Stability of shape in heat treatment	A	
Machinability	E	
Hot hardness	C	
Wear resistance	B/C	
Toughness	E	

The die, punch, mandrel, and expanding post are coated in a thermal diffusion process, which is a typical coating process for blanks, dies, and components used in similar high stress forming operations. The coating provides additional lubricity and reduces reactionary stresses during extrusion. Additionally, the tool toughness and hardness are promoted, and in general, the life of the components are extended. The coating data is tabulated in Table 4.

The die, punch, mandrel, and expanding post are coated in a thermal diffusion process, which is a typical coating process for blanks, dies, and components used in similar high stress forming operations. The coating provides additional lubricity and reduces reactionary stresses during extrusion. Additionally, the tool toughness and hardness are promoted, and in general, the life of the components are extended. The coating data 10 of 25 tabulated in Table 4.

Table 4. Oction data for dien andred up the Andrew papains posts [64].

Result Result
5.08-7.62
5.08 2 762 2000
3500–3800
$0.08 \stackrel{0.08}{-}$
Vanadium carbide

4. Materials 4. Materials

The initial aluminum tube (Ø25.40 mm × 1.65 mm) is 6061 per ASTM B210 and the The initial aluminum tube (Ø25.40 mm × 1.65 mm) is 6061 per ASTM B210 and the initial copper tube (Ø28.58 mm × 1.65 mm and Ø25.40 mm × 1.65 mm) is C12700 per ASTM B75. The true stress-strain curves of the materials, after initial annealing, are presented in F15. The true stress-strain curves of the materials, after initial annealing, are presented in F15. The true stress-strain curves of the materials after initial annealing, are presented in F15. F16 true stress were determined per ASTM E8 using the bulk tube as the specimen. F19 Tigure 5. F16 curves were determined per ASTM E8 using the bulk tube as the specimen.

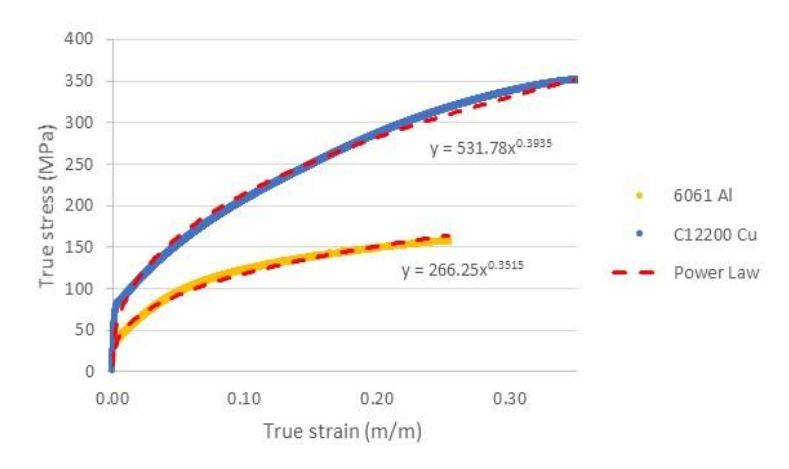


Figure 5. True stress-strain curves of annealed copper and aluminum. Material behavior is modeled **Figure 5.** True stress-strain curves of annealed copper and aluminum. Material behavior is modeled by the power law. eled by the power law.

Before processing, the as-received material is annealed since the aluminum and copper were tempered to T6, and H58, respectively. Both initial annealing cycles were performed as recommended by the Society of Manufacturing Engineers to produce optimally ductile materials as previously described. To confirm the effectiveness of the initial annealing, hardness measurements were taken; the results are shown in Table 5. The copper experienced a 60.2% decrease in hardness and the aluminum experienced a 67.8% decrease. Knoop hardness testing was performed using a 500 g force held for 10 to 15 s where the hardness value was averaged over 10 samples.

Table 5. Hardness of mill and annealed material (HK).

Material	Mill	Annealed
Copper	141.1	56.1
Aluminum	126.4	40.7

The copper and aluminum material behavior are fitted with the power law with an R^2 value of 0.9816, and 0.9893, respectively. Figure 5 shows that the copper and aluminum exhibit strain-hardening which is represented well by the power hardening law shown in Equation (1):

$$\sigma = K\varepsilon^n \tag{1}$$

The strength coefficient, *K*, and the strain hardening exponent, *n*, are presented in Table 6. An important item of note is the dissimilarity between both materials true stress-strain curves. For consistent plasticity to occur within both metals, and to maintain balanced layer formation, similar flow stress behavior across the material is tactically sought; however,

Metals **2021**, 11, 389 11 of 25

the copper has a strength coefficient 99.7% larger than the aluminum, which is expected to influence the difference between extruded layer thicknesses. The values of the strain hardening exponent represent how quickly the material hardens when deforming. A value closer to zero represents a material resisting deformation, while the values closer to one represent a material where true stress and true strain vary proportionality.

Table 6. Power law strength coefficient and exponent.

Strength Coefficient <i>K</i> , MPa	Strain Hardening Exponent n
531.78	0.3935 0.3515
	K, MPa

The extrusion process is modeled in ANSYS Mechanical (ANSYS 19.1., ANSYS Soft-

5. Finite Element Method-Based Simulations of Extrusion

ware Company, Canonsburg, PA, USA) to gain insight on the plastic behavior of the bimetal and to understand the stresses that develop within the die. The geometry of the extrusion model consists of four components: Two metals experiencing extrusion and two workpieces enabling the extrusion. The two metals are referred to as the outer and inner metals, which represent the initial outer, and inner diametrical layers, respectively. For all simulations and experiments, the copper is always the outermost metal tube. The model is axisymmetric and 2-dimensional. Figure 6a shows the ANSYS model of the Metals 2021, 11, x FOR PEER REVIEWextrusion process, where axis symmetry is taken about the farthest left edge. The geometraly represents a 2-dimensional "slice" of the area-of-interest, which is the lower section of the die and mandrel identified by the red circle in Figure 6b. The model is axisymmetric and 2-dimensional because no 3-dimensional instead are written stress or strain convergence duration. The other plantage is precision processed in the die written by the red circle in Figure 6b. The model is axisymmetric and 2-dimensional plantage in the red circle in Figure 6b. The model is axisymmetric and 2-dimensional plantage in the red circle in Figure 6b. The model is axisymmetric and 2-dimensional plantage in the red circle in Figure 6b. The model is axisymmetric and 2-dimensional plantage in the red circle in Figure 6b. The model is axisymmetric and 2-dimensional plantage in the red circle in Figure 6b. The model is axisymmetric and 2-dimensional plantage in the red circle in Figure 6b.

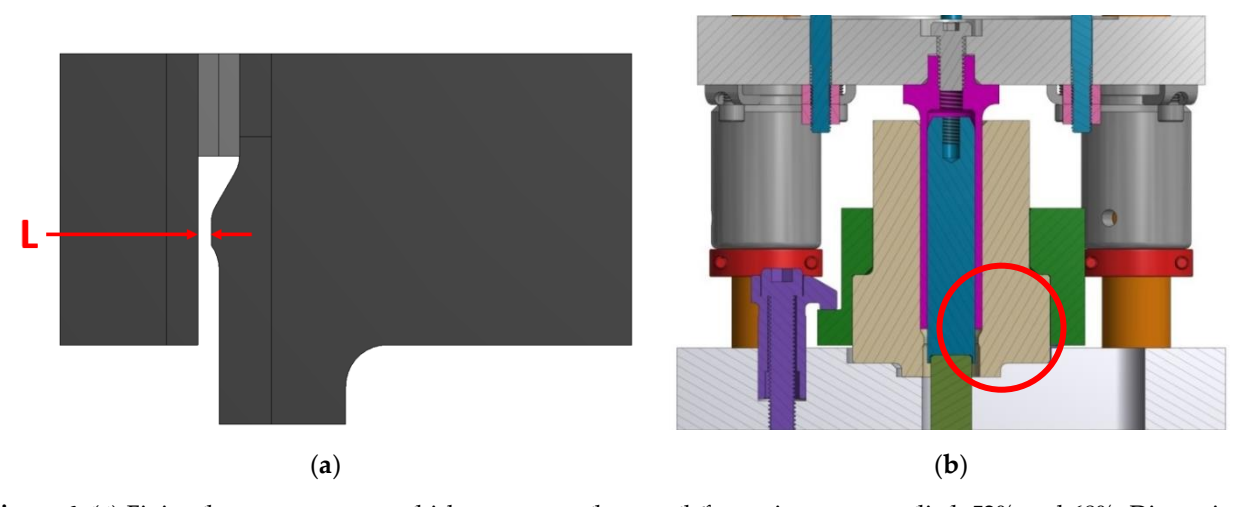


Figure 6. (a) Finite element geometry which represents the two deformation cases studied: 52% and 68%. Dimension L was adjusted to obtain the two different cases. (b) The experimental setup is shown at dead-bottom position, where the simulated area is identified by a red circle.

The geodeltis partitified interestions are contained and assistions the borroriginal growth textusions problems of the situation the inches and the contained and the containe

The model is partitioned into various sub-sections of the original geometry to focus higher element density to the area of interest which is the internal edges of the mandrel

Bimetal

Figure 6. (a) Finite element geometry which represents the two deformation cases studied: 52% and 68%. Dimension L was adjusted to obtain the two different cases. (b) The experimental setup is shown at dead-bottom position, where the Metalinan days are directed.

12 of 25

The model is partitioned into various sub-sections of the original geometry to focus higher element density to the area of interest which is the internal edges of the mandrel and dide: The model is shown in Figure 7. After performing a mesh sensitivity satisfy the model includes 26,286 the month with 75,7885 noodes.

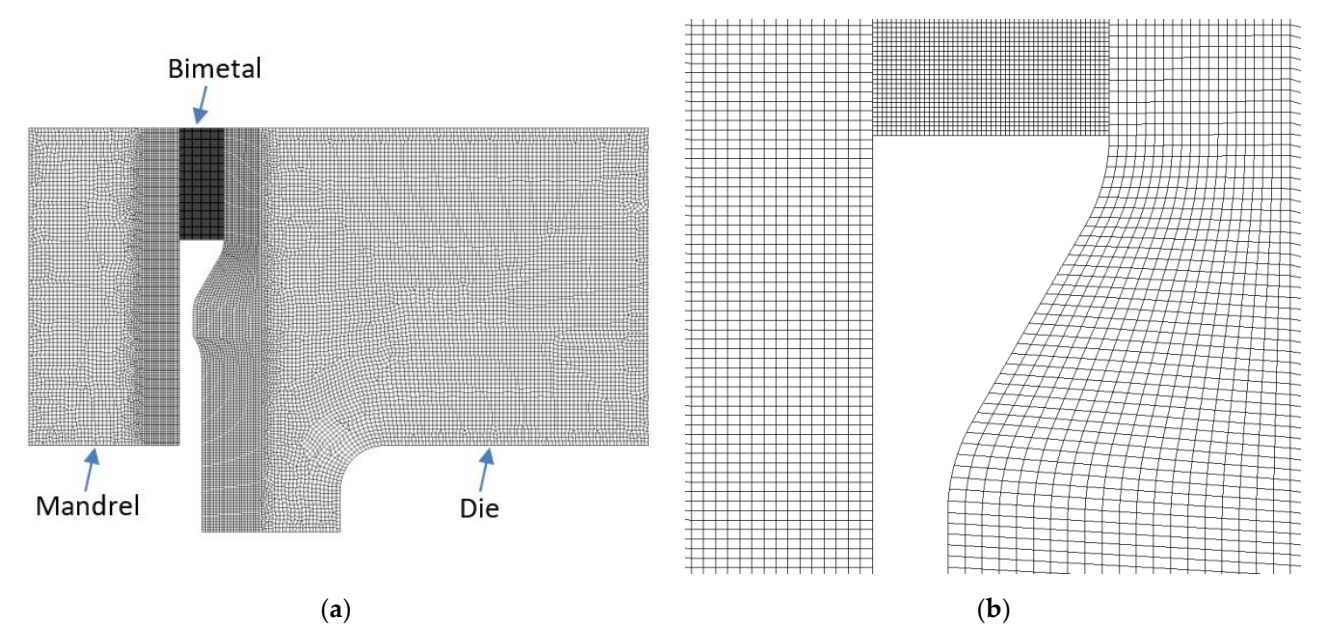


Figure 7.(4) Three structum model meshing, and (b) close-up of the meshing, where the medial attack will expresize exerts $\tan a = a + b$. In the diagled a = a + b.

The controlled with an augmented LaGrange formulation with motal roomal to tagget dectation metabled with an augmented LaGrange formulation with motal roomal to tagget dectation metabled. He considered dectation metabled with a computational departs afty longengely solive three don't colored be described and an augmented dectation with a computational departs afty longengely solive three don't colored be decided by the control of the dectation with a computational departs and decided by the control of the dectation of the decta

An input displacement of 7.62 mm is applied to the top surfaces of the metals experiencing extrusion which forces them to interact with the extrusion ledge as shown. The input of 7.62 mm is used, as this is sufficient displacement to achieve steady-state plastic flow during the extrusion simulation.

The die and mandrel are evaluated for yielding in four instances where copper-copper and copper-aluminum bimetals are extruded at 52% and 68% deformation. Results are shown in Figure 8. Peak stress occurs on the 30° ledge of the die when extruding copper-copper at 68% deformation where a maximum Von Mises stress is found to be 955 MPa. This demonstrates that a factor-of-safety of 1.7 is achieved in the most stressed condition with the yield strength of 1600 MPa estimated for the die material. Because of this, neither mandrel nor the die are expected to yield. As shown in previous research, a 30° die angle is optimal when compared to 22.5, 45, and 60° angles of similar die design for reducing peak stresses [31].

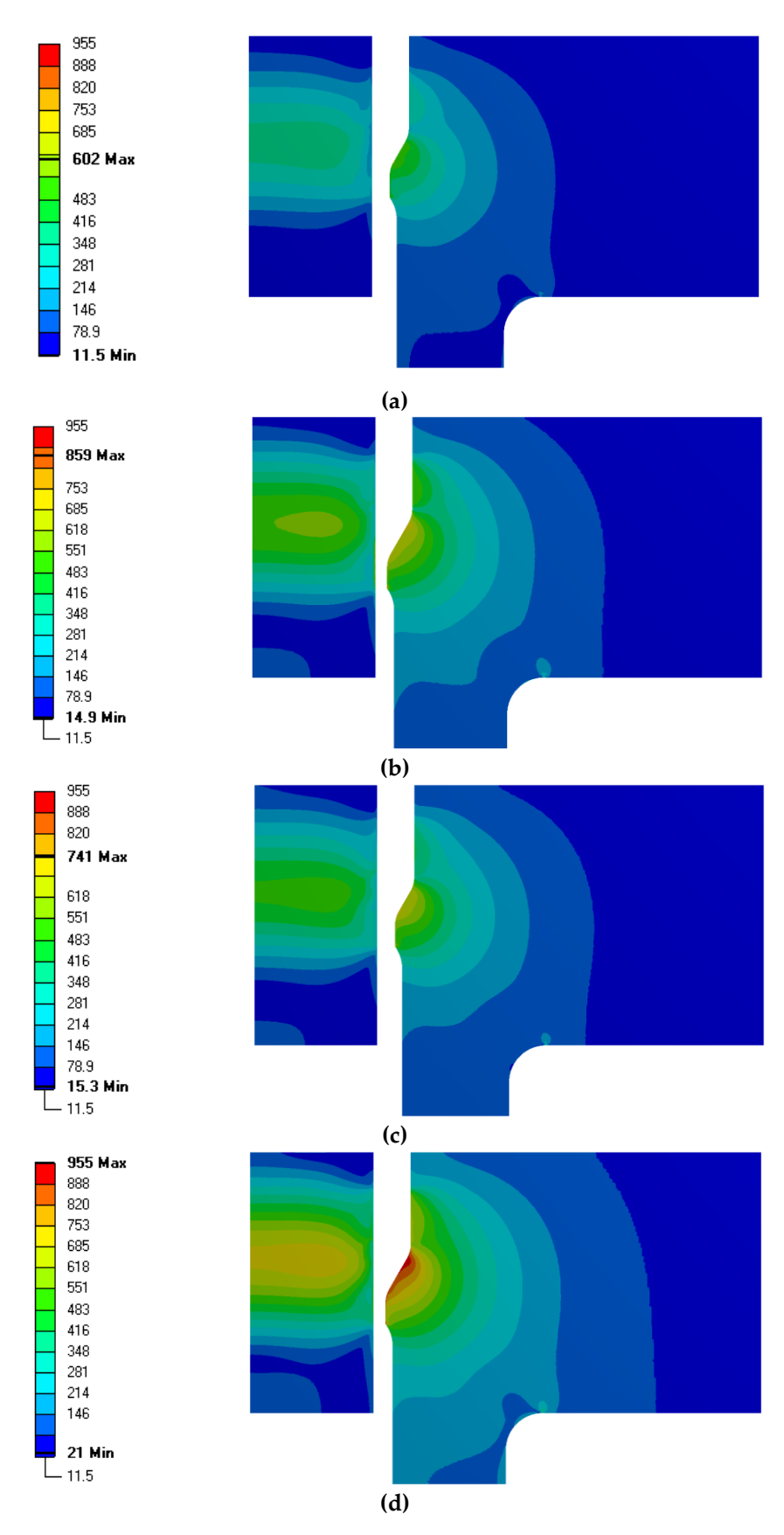


Figure 8. Von Mise Fistress within Mise stime advantantien of supposed and supposed

Metals 2021, 11, 389

Steady-state extrusion begins after 4 mm of punch displacement. The force, found at 4.4 mm, is 167 kN as shown in Figure 9 for the copper-coppe Beyond this peak, the input force decreases linearly with a slight negative Steady-state extrusion begins after 4 mm of punch displacement. The peak input bimetal is within the displacement with a slight negative bimetal is within the displacement of the copper-saluration with bilinetal where linear linea

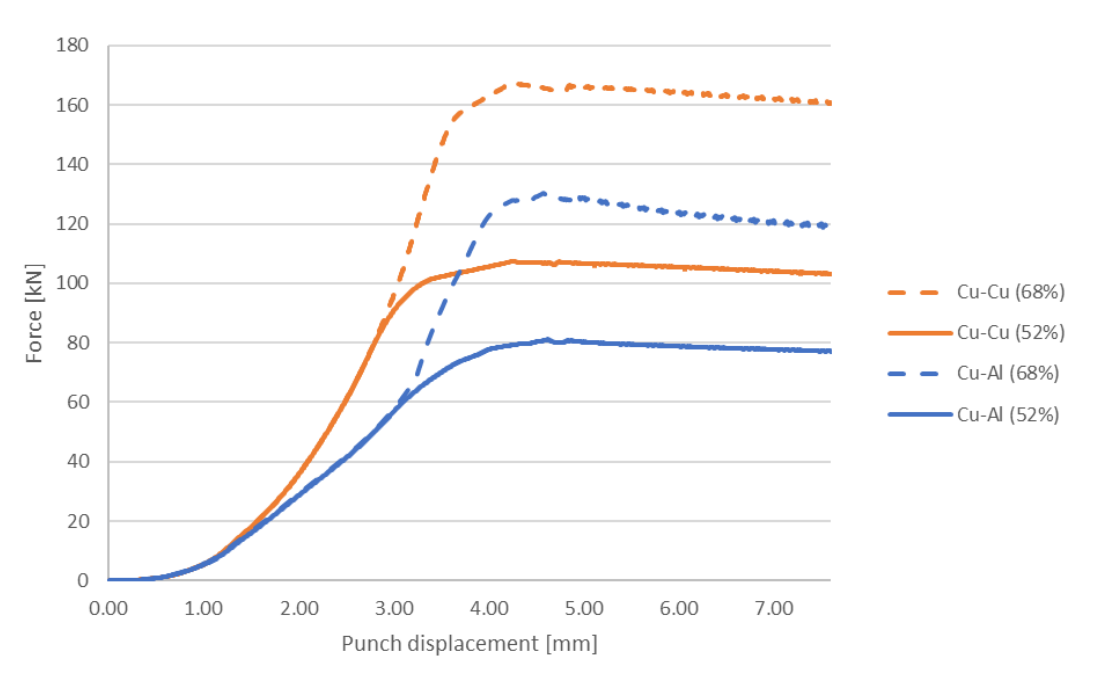


Figure 9. Force-displacement curve for extrusion at 52% and 68% deformation for copper-copper Figure 9per-aluminum himetals.

and copper-aluminum bimetals.

As the bimetals pass the extrusion ledge, a significant amount of plastic deformation occurs. The resultant total plastic deformation is shown in Figure 10 for all four cases. In the session that invertals plastic state plastic strains are the session of the plastic strains of the session of the plastic strains of the session of the tube and decreases close the shearth to the mappines by order the plastic strain is found on the innermost edge of the tube and decreases close the shearth to the mappines by order the plastic strain is greatly to the mappines by order the plastic strain is greatly to the mappines by order the plastic strain is greatly to the thickness and bimoet al. the hower time figure feelth is the plastic strain in the inner metal. This is observed in all four closes, and peaceful to the mappines for the plastic strain in the inner metal. This is observed in all four closes, and peaceful to the mappines of the outer metal causing more strain in the inner metal. This is observed in all four closes, and peaceful interfered the course of the outer metal causing more strain in the inner metal. This is observed in all four closes, and peaceful interfered to the mappines of the outer metal causing more strain in the inner metal. This is observed in all four closes, and peaceful interfered to the mappines of the outer metal interfered to the outer of the outer metal interfered interfered to the outer of the outer of the metal-metal interfered interfered to the outer of the outer of the metal-metal interfered interfered to the outer of the metal-metal interface. So 1% for copper-dumining when he deformation is increased in outer of the oute

Producing the tubes in this manner requires sacrificing the beginning are extruded tubes. As is evident, the initial section does not fully achieve plastic and the end section is not pressed fully past the extrusion ledge.

Metals 2021, 11, x FOR PEER REVIEW 16 of 27

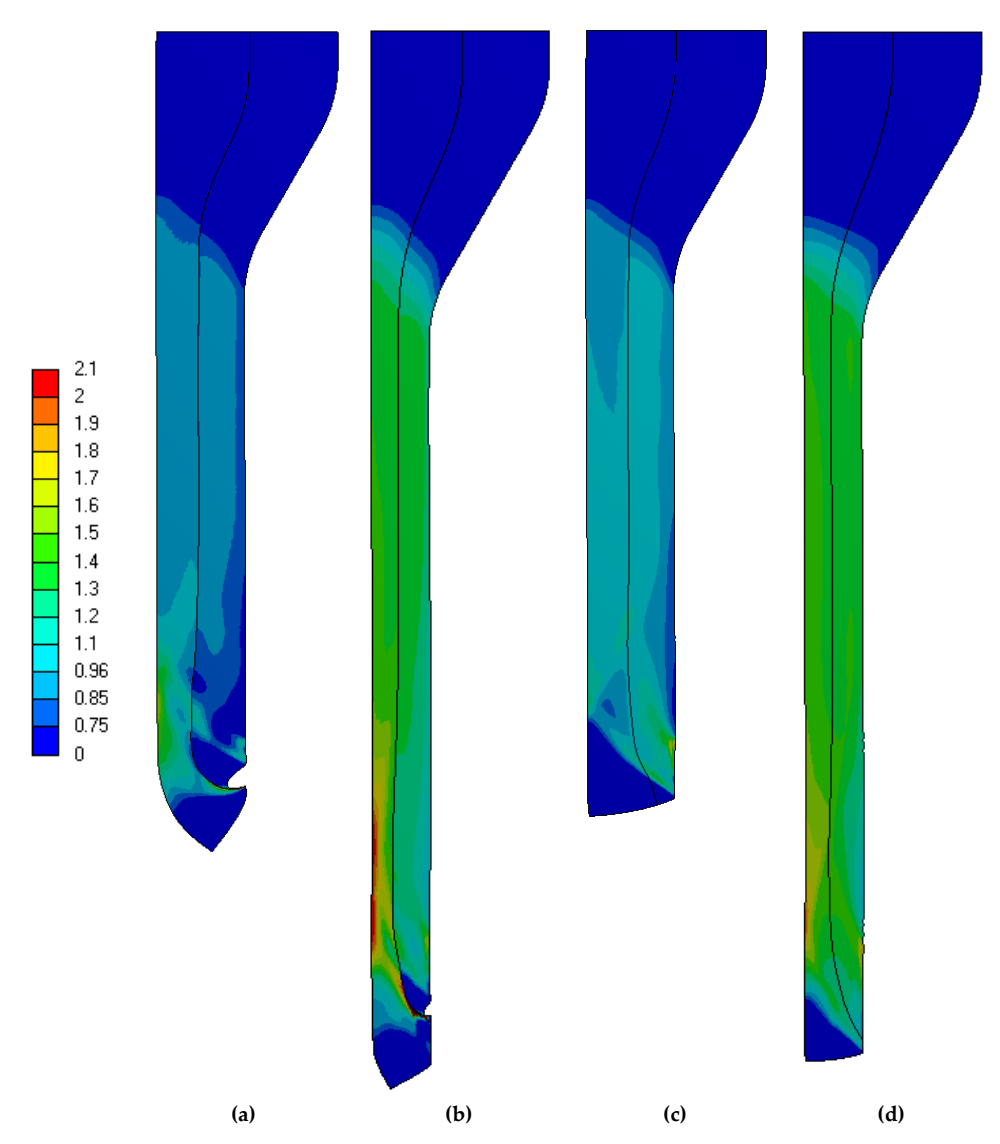


Figure 10. Total aguivalent plastic strain at 762 mm of displacement for copper-aluminum at (a) 52%, and (b) 68% deformation. The die and mandrel are omitted. Units of strain are 17 of 27 deformation and mandrel are omitted. Units of strain are 17 of strain are 18 of strain are 19 of strain are

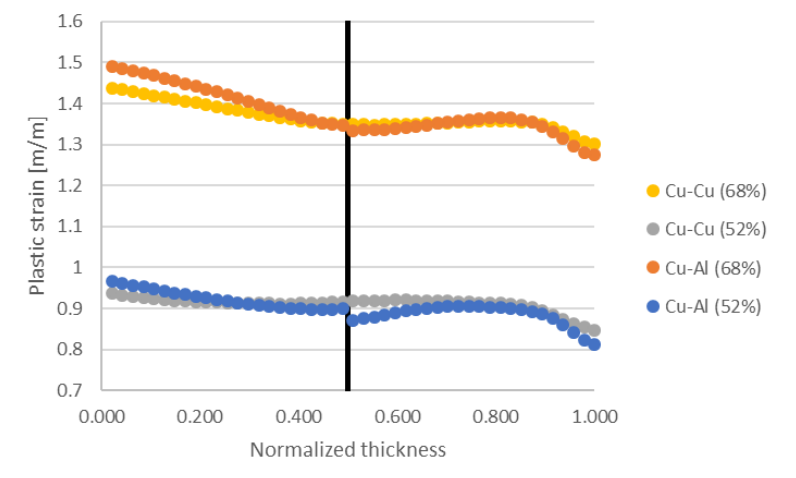


Figure 11. Equivalent plastic strain through the extruded wall where normalized 0.0 is the inner Figure 30 of the training particular through the extruded wall where normalized 0.0 is the inner Figure 30 of the training particular through the extraction of the content of the content of the extruded bimetal. Sents bonding interface location. Plastic strain is taken at the vertical midpoint of the extruded bimetal.

6. Results and Discussion

Copper-copper and copper-aluminum bimetallic tubes were produced using the

Metals **2021**, 11, 389 16 of 25

Producing the tubes in this manner requires sacrificing the beginning and end of the extruded tubes. As is evident, the initial section does not fully achieve plastic deformation and the end section is not pressed fully past the extrusion ledge.

6. Results and Discussion

Copper-copper and copper-aluminum bimetallic tubes were produced using the methodology described. The initially stacked copper-copper and copper-aluminum tubes were measured to have an average outer diameter of 28.58 mm and an inner diameter of 22.1 mm before processing. After the AEB process, the outer diameters were reduced to an average of 25.324 mm for the 52% extrusion and 24.257 mm for 68% extrusion. For all extrusions, the inner diameters were found to be 22.073 mm on average. This demonstrates that 49.9% and 66.3% radial deformation was achieved which is less than the targeted 52%, and 68% deformation, respectively. This is due to initial air gaps between the stacked layers, the mandrel, and the die, as well as expansion of the die during extrusion.

Table 7 summarizes all bimetallic tubes produced and whether bonding was achieved or not. The copper-copper tube serves as a baseline and represents the easiest possible chance to achieve full-bonding since metallographic substructures are consistent and the material exhibits identical material behavior. Copper-aluminum, however, represents a combination that is more difficult to bond due to differences in material behavior and different naturally occurring oxide layers. Four-layer tubes of copper-copper, and higher, were not attempted since the 2-layer copper-copper tube demonstrates that bonding is possible using AEB. Further processing of a copper-copper tube would provide no more desired insight as future iterations are expected to bond as the first 2-layer.

Table 7. Summary of bimetallic tubes produce	ble 7. Su	mmary o	of bimet	allic tubes	produced
---	-----------	---------	----------	-------------	----------

52% Def	ormation	
2-layer	4-layer	8-layer
Yes *	Yes*	Yes *
Yes *		
68% Def	ormation	
2-layer	4-layer	8-layer
Yes		
	2-layer Yes * Yes * 68% Def	Yes * Yes * Yes * 68% Deformation 2-layer 4-layer

^{* =} no bonding.

Despite adhering to the methodology described above, all samples extruded at 52% did not bond. The only successful bonding occurred at 68% deformation in the coppercopper bimetallic tube. Based on the extrusions performed, deformation greater than 52% is required for bonding since the processing remained constant between all tests. The processing of the 8-layer copper-aluminum tube demonstrates that the extrusion and expansion process can create bimetallic tubes, but deformation percentage needs to be of sufficient strain to enact bonding as shown in the 68% deformed copper-copper tube. Most literature in ARB reports 50% as the low-end of deformation required to enact bonding. Evidently, bonding in the AEB process did not occur at 50% revealing the role of more complex geometry of tube relative to sheet. Mechanical fields in the tube during AEB are different than those in the sheet during ARB making the strain levels required for bonding greater in AEB process than in ARB process.

The copper-aluminum bimetal tube cross-section, shown in extrusion direction, is displayed in Figure 12. As shown in this paper, the layer thickness decreased exponentially, while the tube wall thickness remained constant. Tabulated in Table 8 are the minimum and maximum layer thicknesses measured at the cross-section taken. The 2-layer bimetal tube has very consistent layer thicknesses as well as the 4-layer bimetal. At 8-layers, the layer thickness varied greatly where some layers completely thinned to obsolesce. Beyond this, layer thickness was very inconsistent in the 8-layer bimetal.

Metals 2021, 11, 389

In each sample produced at 52% deformation, bonding did not occur and is observed as the dark voids at each interface, as shown in Figure 12. Each subsequent extrusion pass did not further promote bonding as observed in the 8-layer bimetal. For this reason, it is necessary to achieve bonding on the first extrusion iteration. Since bonding did not occur, the material layers acted independently for each future extrusion, and the thin layers did of 25 not handle the imposed plastic strain, which ultimately caused significant wrinkling and tearing on the innermost and outermost layers, as well as layer thinning inside the bimetal.

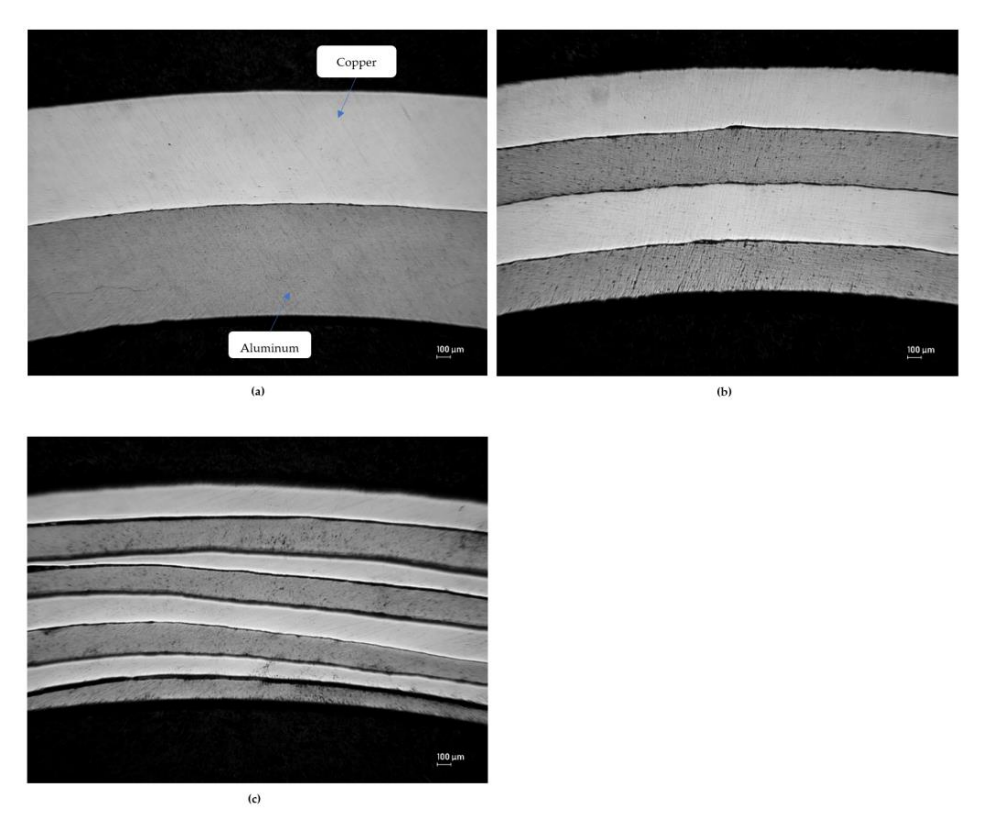


Figure 12. Dimetallisa who of a 12 2 week by 14 4 year, and (3) Extry coproporting invariant who who in the extrusion direction, produced a \$32% deformation.

Table 8. Minimum and maximum layer thickness (μm) at 52% deformation.

Layers	!	2	4	1	8	3
Material	Cu	Al	Cu	Al	Cu	Al
Expected	794	794	396	396	198	198
Average	819	775	414	375	212	200
Minimum	802	743	385	349	0	0
Maximum	847	798	462	402	440	504

In each sample produced at 52% deformation, bonding did not occur and is observed as the dark voids at each interface, as shown in Figure 12. Each subsequent extrusion pass did not further promote bonding as observed in the 8-layer bimetal. For this reason, it is necessary to achieve bonding on the first extrusion iteration. Since bonding did not occur, the material layers acted independently for each future extrusion, and the thin layers did not handle the imposed plastic strain, which ultimately caused significant wrinkling and tearing on the innermost and outermost layers, as well as layer thinning inside the bimetal.

Copper-copper bimetallic tubes were attempted at both 52% and 68% deformation. As mentioned previously, no bonding was achieved at 52% deformation when attempting a copper-copper bimetal. However, using the same method described, bonding was achieved using 68% deformation. As shown in Figure 13, the 2-layer copper-copper bonded interface is observed normal to the extrusion direction. Unlike Figure 12, the copper-copper cross section, shown in Figure 13, required acid-etching to view the interface using microscopy. The layer thickness was measured and found to be 510 µm for the outer layer of copper and 568 μ m for the inner layer of copper where the expected thickness was 527 μ m. This is attributed to the outer layer being pulled in front of the extrusion ledge during the initial extrusion start which is exhibited predominantly in Figure 10a,b.

Metals 2021, 11, 389

achieved using 68% deformation. As shown in Figure 13, the 2-layer copper-copper bonded interface is observed normal to the extrusion direction. Unlike Figure 12, the copper-copper cross section, shown in Figure 13, required acid-etching to view the interface using microscopy. The layer thickness was measured and found to be 510 µm for the outer layer of copper and 568 µm for the inner layer of copper where the expected thickness was 527 µm. This is attributed to the outer layer being pulled in front of the extrusion ledge during the initial extrusion start which is exhibited predominantly in Figure 10a,b.

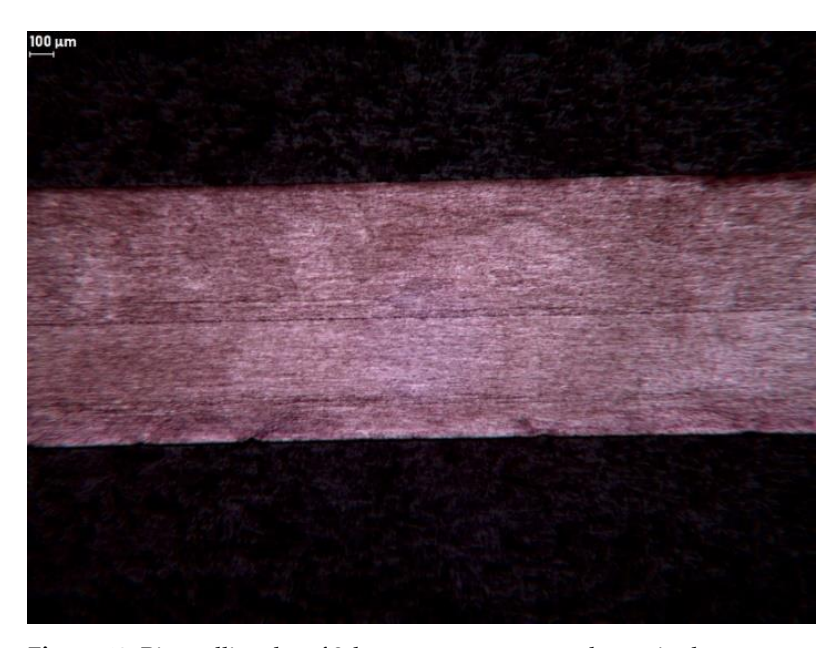


Figure 13. Bimetallic tube of 2-layer copper-copper, shown in the transverse direction, produced at 68% deformation.

Full bonding, however, dichord occur as there are voids at the interface. A 15,240 µm longs ection was survey echandes 50% of the length was found to be bonded. In this section, 148 voids were identified with an average length of 15,44 µm. No identifiable pattern was observed aganding the black tion of the boxs, dia and the described was found to be 49.7 µm. Metals 2021, 11, × FOR PEER REVIEW, pical and the overhowing in Figural which which presente syntack a black at the cinterface.

Violate and the presentations are the presented to the contractions.

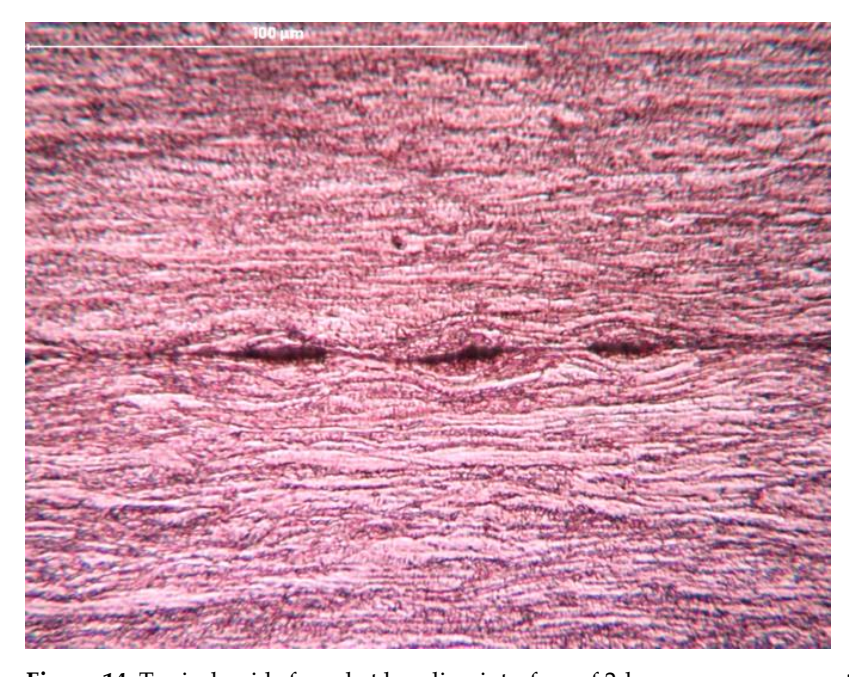


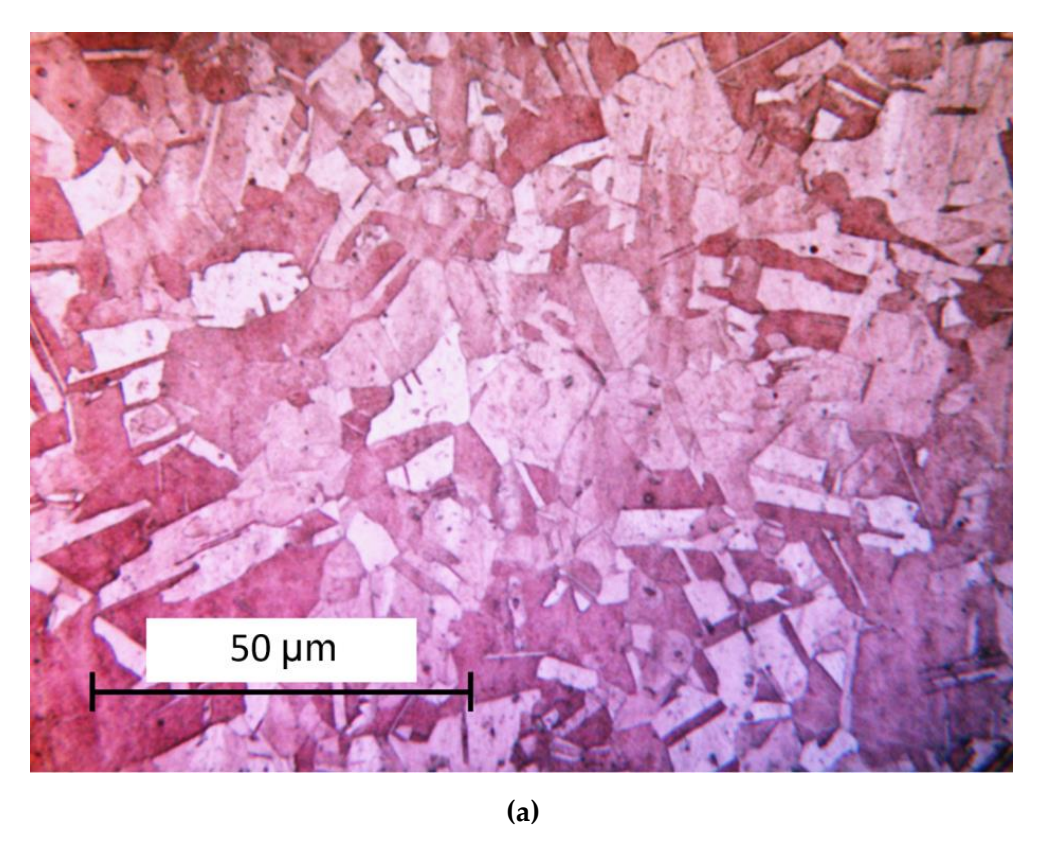
Figure 14. Typical voids found at bonding interface of 2-layer copper-copper tube shown in transverse yerse direction. Bimetal was extruded at 68% deformation.

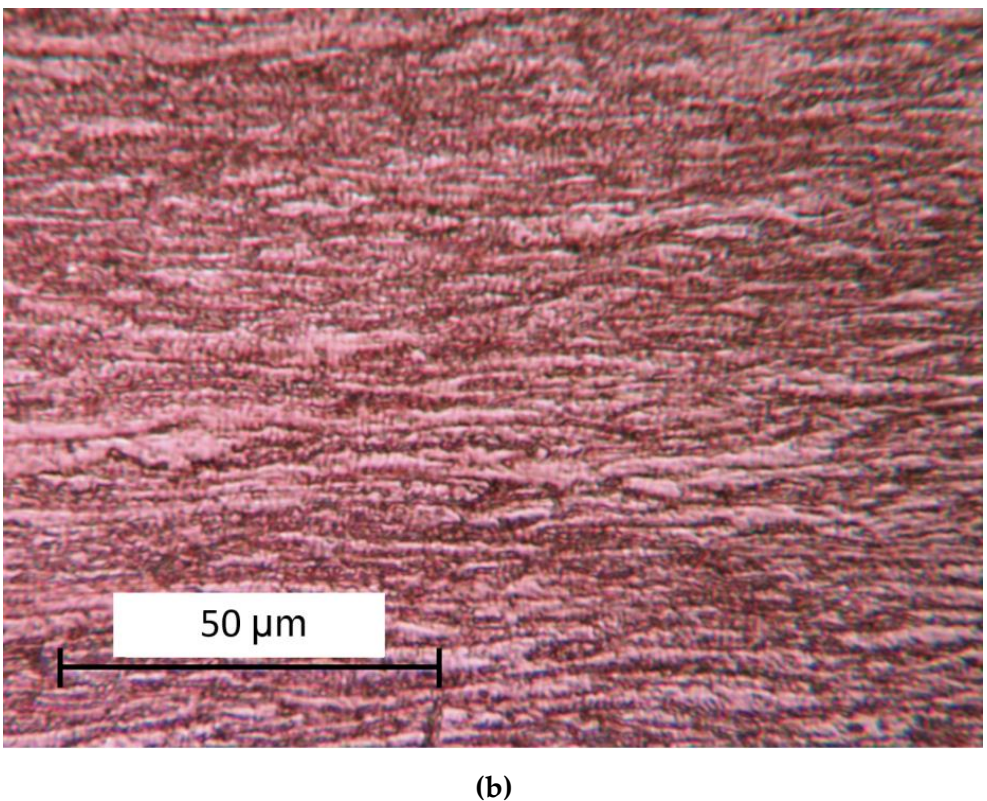
The grain structure before and after extrusion is displayed in Figure 15. As how in the transverse direction the envaled grain structure because high wighny entergated on the tox true in the inventor of the extrusion of the inventor of the extrusion of the partial behavior where grains no longer have uniformity in all spatial directions, which is expected for non-heat-treated metal after drawing or extrusion.

Metals **2021**, 11, 389 19 of 25

Metals 2021, 11, x FOR PEER REVIEW

an anisotropic material behavior where grains no longer have uniformity in all spatial directions, which is expected for non-heat-treated metal after drawing or extrusion.





FigureFig. Mail-Fo-Microstructure of perpera (b) before entrusion, and (b) after extrusion as 68 %8 % denotion at in.

The copper-aluminum and copper-copper bimetal underwent signification hardening during extrusion at 52% and 68% deformation. As tabulated in Table 10, the hardness of each metal constituent increased significantly. The 8 per-aluminum was not tested for hardness since the individual layers were to

Metals **2021**, 11, 389 20 of 25

The copper-aluminum and copper-copper bimetal underwent significant strain-hardening during extrusion at 52% and 68% deformation. As tabulated in Tables 9 and 10, the hardness of each metal constituent increased significantly. The 8-layer copper-aluminum was not tested for hardness since the individual layers were too small for micro-hardness testing. Interestingly, the copper-copper layers experienced approximately the same increase (165.1% vs. 168.5%) in hardness even though the deformation percentage was 52% and 68% respectively. This suggests there is a hardening limit as no significant increase in hardness was observed with strain.

Table 9. Hardness (HK) before and after extrusion of 2-layer copper-copper bimetal.

Deformation	Annealed	2-Layer	Increase (%)
52%	56.1	148.8	165.1
68%	56.1	150.7	168.5

Table 10. Hardness (HK) before and after extrusion of copper-aluminum bimetal at 52% deformation.

Material	Annealed	2-Layer	Increase (%)	4-Layer	Increase (%)
Copper Aluminum	56.1 40.7	144.0 72.8	156.6 78.9	146.9 71.8	161.9 76.4
Alullillulli	40.7	72.0	76.9	71.0	70.4

The copper-copper tube, extruded at 68%, exhibits significantly improved material strength as indicated by the material behavior displayed in Figure 16. A second tensile test was performed to confirm results; a difference of ~2% was identified between the two ultimate tensile strengths found. Tensile tests were performed per ASTM E8 using custom sidewall specimens. The 0.2% offset yield strength improved from 83 MPa to 481 MPa; a 480% increase compared to the annealed material. Due to the work hardening experienced during extrusion, ductility is sacrificed for the improved material strength.

The ultimate tensile strength of the copper-copper tube, extruded at 68% using AEB, is compared to pure copper experiencing ARB, as reported by [70], and tube cyclic extrusioncompression (TCEC), as reported by [71]. TCEC is a severe plastic deformation technique where tubes are fully constrained and deformed between an external chamber and an internal mandrel [71]. The pure copper undergoing ARB and TCEC achieved ultrafine grain size after four passes of severe plastic deformation processes. Pure copper experiencing 68% AEB, on the other hand, has a grain size approximately one order of magnitude greater but exhibits the greatest improved ultimate tensile strength in one iteration. The significant improvement of strength is attributed to the hyper-elongated grains shown in Figure 15b, which are oriented in the extrusion direction, where dislocation structures, and underlying residual stress fields expected to form during the process similar to ARB [72]. We observe that grain size obtained is an order of magnitude larger than other severe plastic deformation processes (Table 11), but the largest improvement in ultimate tensile strength was obtained. Therefore, grain size refinement alone does not govern improvements in material strength, but also other features such as dislocation density and low angular boundaries in sub-grain structure also impact strength. Anisotropic material properties are expected since the average grain size is 2.3 µm in the extrusion direction and an average length of 40 μm is in the transverse direction.

Metals **2021**, 11, 389 21 of 25

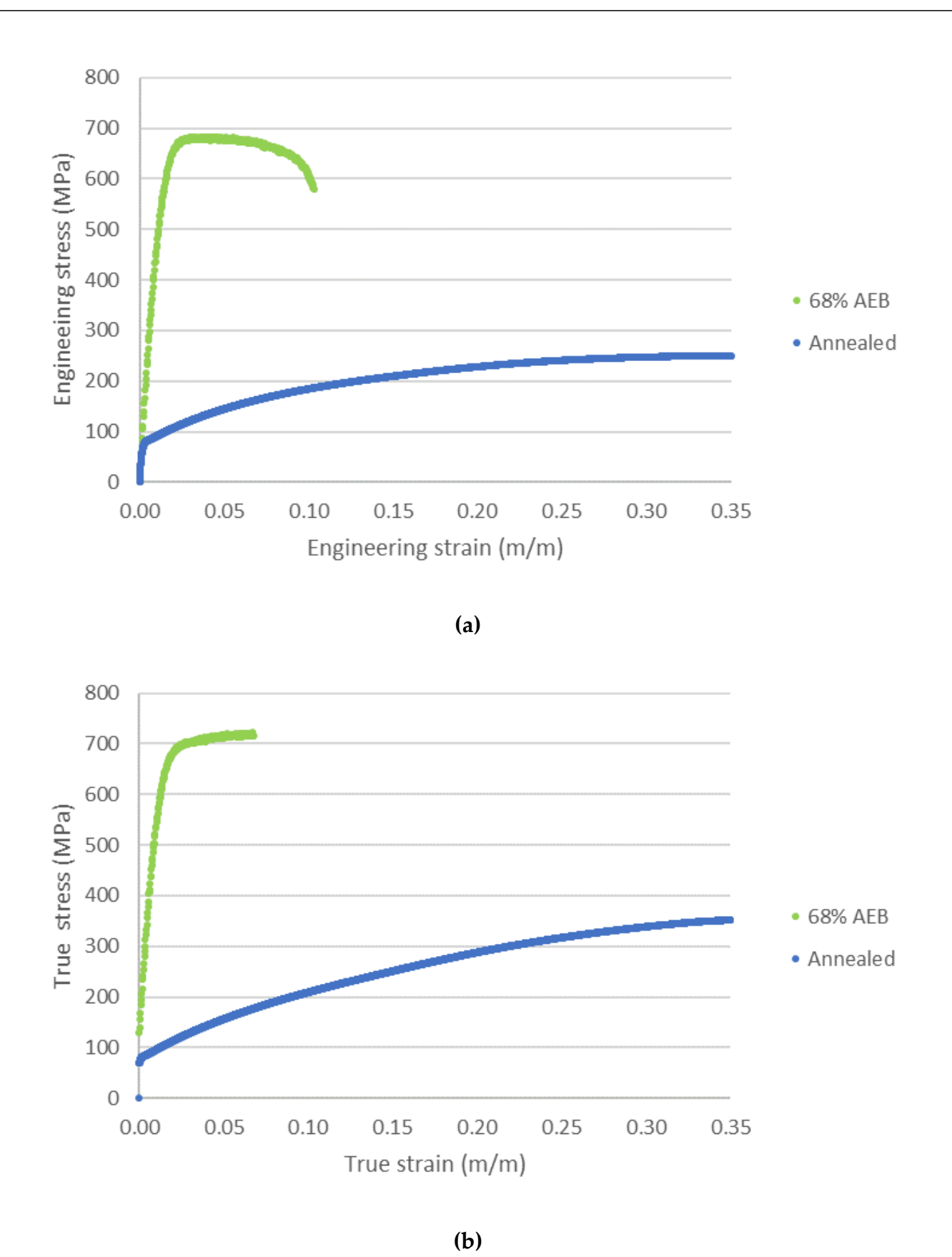


Figure 16. EisyméerFingistresisestram, stainante inderstressessitamin, (b) of 68% deferontiation 2016 year copper copper coppered impared to annealed curves.

The ultimate tensile strength of the copper-copper tube, extruded at 68% using AE is compared to pure copper experiencing ARB, as reported by [70], and tube cyclic extr sion-compression (TCEC), as reported by [71]. TCEC is a severe plastic deformation tecnique where tubes are fully constrained and deformed between an external chamber an internal mandrel [71]. The pure copper undergoing ARB and TCEC achieved ultrafi

Metals **2021**, 11, 389 22 of 25

able 11. Ultimate tensile strength of pure copper deformed using different severe plastic deformation
rocesses.

Process	Iteration	Ultimate Tensile Strength (MPa)	Percent Difference to Annealed (%)
68% AEB	1	683	172%
ARB [70]	1	350	39%
ARB [70]	2	370	47%
ARB [70]	3	395	57%
ARB [70]	4	395	57%
TCEC [71]	1	275	10%
TCEC [71]	2	300	20%
TCEC [71]	3	310	24%
TCEC [71]	4	325	29%
Annealed	-	251	0%

7. Summary and Conclusions

This work developed a process termed accumulative extrusion bonding for introducing laminated structures in metallic tubes. To this end, dies are designed and evaluated using the finite element method simulations. Several multilayered tubes are produced using the process and characterized for the extent of bonding, microstructure, hardness, and strength. Significantly, bonding at the interface is achieved for the copper-copper metallic tubing to about 85% at a radial strain of 68% imparted by the AEB process. Since complete bonding is desired, it is recommended to increase the radial deformation to a value greater than 68%. The additional key findings are:

- 1. Bonding using AEB does not occur at 50% deformation revealing the significant role of more complex geometry of tubes relative to sheets in solid-state bonding. Mechanical fields in the tube during AEB are different from those in the sheet during ARB making the required strain levels for bonding greater in AEB process than those in ARB process.
- 2. It is necessary to achieve bonding on the first extrusion pass/iteration as future extrusion passes would not promote bonding. Since bonding does not occur on the first extrusion pass at 52% deformation, the material layers act independently for each future extrusion. Moreover, the layers begin to lose their integrity with plastic strain.
- 3. Surface preparation before forming the interface is very important to facilitate bonding using AEB. Any imperfection left on the interfacial layer will become an inclusion at the interface. During processing it is therefore critical to minimize inadvertent mishandling or extraneous debris. Further processing will thin and stretch areas of contamination but will not remove the inclusions. Moreover, oxidation layer minimization is necessary to aid in bonding. Scratch brushing is used as the process to promote surface hardening while also aiding in the removal of any oxide layer. This method also does not produce any noticeable debris from the bristles which helps promote cleanliness. It is found that over-brushing does not improve the amount of bonding. Beyond scratch brushing, which is a key application to remove oxides and encourage surface hardness, minimizing contact with the atmosphere is also essential.
- 4. Annealing during each iteration is necessary to remove strain hardening caused during extrusion. Samples extruded with the annealing step omitted failed during extrusion due to wrinkling and tearing.

To achieve unique material properties permitted by ultrafine-laminated structures in tubes like those achieved in sheets, it is necessary to bond different material combinations and further push the layering to the thickness at and below the grain size-level. Future work will explore the possibility to extrusion bond more metal-metal combinations, push the processing to achieve finer layering, and, as necessary, improve the die design.

Metals **2021**, 11, 389 23 of 25

Author Contributions: Conceptualization, M.R.S. and M.K.; methodology, M.R.S. and M.K.; writing—original draft preparation, M.R.S.; writing—review and editing, M.K. Both authors have read and agreed to the published version of the manuscript.

Funding: This research was funded by the U.S. National Science Foundation (NSF) under Grant No. CMMI-1727495.

Data Availability Statement: The data presented in this study are available on request from the corresponding author. The data cannot be shared at this time due to technical or time limitations.

Acknowledgments: University of New Hampshire for laboratory support and L&S Machine Company LLC for manufacturing die components. The authors also acknowledge support and input from professors Brad L. Kinsey, Jinjin Ha, and Yannis P. Korkolis.

Conflicts of Interest: The authors declare no conflict of interest.

References

- Bimetallic Tubes. Available online: http://www.beca-engineering.com/product/bimetallictubes.php (accessed on 12 January 2021).
- 2. Bimetallic Tubes. Available online: https://www.dmitubes.com/bimetallic-tubes.html (accessed on 12 January 2021).
- 3. New Generation Bimetallic Tubes. Available online: https://www.energetictubes.com/ (accessed on 12 January 2021).
- 4. Bimetallic Tubes. Available online: https://www.materials.sandvik/en-us/products/tube-pipe-fittings-and-flanges/tubular-products/bimetallic-tubes/ (accessed on 12 January 2021).
- 5. Hosseini, M.; Pardis, N.; Manesh, H.D.; Abbasi, M.; Kim, D.-I. Structural characteristics of cu/ti bimetal composite produced by accumulative roll-bonding (arb). *Mater. Des.* **2017**, *113*, 128–136. [CrossRef]
- 6. Jamaati, R.; Toroghinejad, M.R. Manufacturing of high-strength aluminum/alumina composite by accumulative roll bonding. *Mater. Sci. Eng. A* **2010**, 527, 4146–4151. [CrossRef]
- 7. Dehsorkhi, R.N.; Qods, F.; Tajally, M. Investigation on microstructure and mechanical properties of al–zn composite during accumulative roll bonding (arb) process. *Mater. Sci. Eng. A* **2011**, *530*, 63–72. [CrossRef]
- 8. Chang, H.; Zheng, M.; Xu, C.; Fan, G.; Brokmeier, H.; Wu, K. Microstructure and mechanical properties of the mg/al multilayer fabricated by accumulative roll bonding (arb) at ambient temperature. *Mater. Sci. Eng. A* **2012**, *543*, 249–256. [CrossRef]
- 9. Mahdavian, M.; Ghalandari, L.; Reihanian, M. Accumulative roll bonding of multilayered cu/zn/al: An evaluation of microstructure and mechanical properties. *Mater. Sci. Eng. A* **2013**, *579*, 99–107. [CrossRef]
- 10. Ghalandari, L.; Mahdavian, M.; Reihanian, M. Microstructure evolution and mechanical properties of cu/zn multilayer processed by accumulative roll bonding (arb). *Mater. Sci. Eng. A* **2014**, 593, 145–152. [CrossRef]
- 11. Knezevic, M.; Nizolek, T.; Ardeljan, M.; Beyerlein, I.J.; Mara, N.A.; Pollock, T.M. Texture evolution in two-phase zr/nb lamellar composites during accumulative roll bonding. *Int. J. Plast.* **2014**, *57*, 16–28. [CrossRef]
- 12. Ardeljan, M.; Beyerlein, I.J.; Knezevic, M. A dislocation density based crystal plasticity finite element model: Application to a two-phase polycrystalline hcp/bcc composites. *J. Mech. Phys. Solids* **2014**, *66*, 16–31. [CrossRef]
- 13. Savage, D.J.; Beyerlein, I.J.; Mara, N.A.; Vogel, S.C.; McCabe, R.J.; Knezevic, M. Microstructure and texture evolution in mg/nb layered materials made by accumulative roll bonding. *Int. J. Plast.* **2020**, *125*, 1–26. [CrossRef]
- 14. Leu, B.; Savage, D.J.; Wang, J.; Alam, M.E.; Mara, N.A.; Kumar, M.A.; Carpenter, J.S.; Vogel, S.C.; Knezevic, M.; Decker, R.; et al. Processing of dilute mg–zn–mn–ca alloy/nb multilayers by accumulative roll bonding. *Adv. Eng. Mater.* **2020**, 22, 1900673. [CrossRef]
- 15. Mashhadi, A.; Atrian, A.; Ghalandari, L. Mechanical and microstructural investigation of zn/sn multilayered composites fabricated by accumulative roll bonding (arb) process. *J. Alloys Compd.* **2017**, 727, 1314–1323. [CrossRef]
- 16. Clemens, B.; Kung, H.; Barnett, S. Structure and strength of multilayers. MRS Bull. 1999, 24, 20–26. [CrossRef]
- 17. Mara, N.; Bhattacharyya, D.; Dickerson, P.; Hoagland, R.; Misra, A. Deformability of ultrahigh strength 5 nm cu/nb nanolayered composites. *Appl. Phys. Lett.* **2008**, 92, 231901. [CrossRef]
- 18. Zhang, X.; Misra, A.; Wang, H.; Shen, T.; Nastasi, M.; Mitchell, T.; Hirth, J.; Hoagland, R.; Embury, J. Enhanced hardening in cu/330 stainless steel multilayers by nanoscale twinning. *Acta Mater.* **2004**, *52*, 995–1002. [CrossRef]
- 19. Ardeljan, M.; Knezevic, M.; Jain, M.; Pathak, S.; Kumar, A.; Li, N.; Mara, N.A.; Baldwin, J.K.; Beyerlein, I.J. Room temperature deformation mechanisms of mg/nb nanolayered composites. *J. Mater. Res.* **2018**, *33*, 1311–1332. [CrossRef]
- 20. Ardeljan, M.; Savage, D.J.; Kumar, A.; Beyerlein, I.J.; Knezevic, M. The plasticity of highly oriented nano-layered zr/nb composites. *Acta. Mater.* **2016**, *115*, 189–203. [CrossRef]
- 21. Su, Y.; Ardeljan, M.; Knezevic, M.; Jain, M.; Pathak, S.; Beyerlein, I.J. Elastic constants of pure body-centered cubic mg in nanolaminates. *Comput. Mater. Sci.* **2020**, *174*, 109501. [CrossRef]
- 22. Knezevic, M.; Zecevic, M.; Beyerlein, I.J.; Lebensohn, R.A. A numerical procedure enabling accurate descriptions of strain rate-sensitive flow of polycrystals within crystal visco-plasticity theory. *Comput. Methods Appl. Mech. Eng.* **2016**, 308, 468–482. [CrossRef]

Metals **2021**, 11, 389 24 of 25

 Knezevic, M.; Kalidindi, S.R. Fast computation of first-order elastic-plastic closures for polycrystalline cubic-orthorhombic microstructures. Comput. Mater. Sci. 2007, 39, 643–648. [CrossRef]

- 24. Jahedi, M.; Ardjmand, E.; Knezevic, M. Microstructure metrics for quantitative assessment of particle size and dispersion: Application to metal-matrix composites. *Powder Technol.* **2017**, *311*, 226–238. [CrossRef]
- 25. Misra, A.; Hoagland, R. Effects of elevated temperature annealing on the structure and hardness of copper/niobium nanolayered films. *J. Mater. Res.* **2005**, *20*, 2046–2054. [CrossRef]
- 26. Bellou, A.; Scudiero, L.; Bahr, D. Thermal stability and strength of mo/pt multilayered films. *J. Mater. Sci.* **2010**, 45, 354–362. [CrossRef]
- 27. Han, W.; Misra, A.; Mara, N.; Germann, T.; Baldwin, J.; Shimada, T.; Luo, S. Role of interfaces in shock-induced plasticity in cu/nb nanolaminates. *Philos. Mag.* **2011**, *91*, 4172–4185. [CrossRef]
- 28. Wei, Q.; Li, N.; Mara, N.; Nastasi, M.; Misra, A. Suppression of irradiation hardening in nanoscale v/ag multilayers. *Acta Mater.* **2011**, *59*, 6331–6340. [CrossRef]
- 29. Zhernenkov, M.; Jablin, M.S.; Misra, A.; Nastasi, M.; Wang, Y.; Demkowicz, M.J.; Baldwin, J.K.; Majewski, J. Trapping of implanted he at cu/nb interfaces measured by neutron reflectometry. *Appl. Phys. Lett.* **2011**, *98*, 241913. [CrossRef]
- 30. Lesuer, D.; Syn, C.; Sherby, O.; Wadsworth, J.; Lewandowski, J.; Hunt, W. Mechanical behaviour of laminated metal composites. *Int. Mater. Rev.* **1996**, 41, 169–197. [CrossRef]
- 31. Knezevic, M.; Jahedi, M.; Korkolis, Y.P.; Beyerlein, I.J. Material-based design of the extrusion of bimetallic tubes. *Comput. Mater. Sci.* **2014**, *95*, 63–73. [CrossRef]
- 32. Valiev, R.Z.; Estrin, Y.; Horita, Z.; Langdon, T.G.; Zechetbauer, M.J.; Zhu, Y.T. Producing bulk ultrafine-grained materials by severe plastic deformation. *JOM* **2006**, *58*, 33–39. [CrossRef]
- 33. Knezevic, M.; Bhattacharyya, A. Characterization of microstructure in nb rods processed by rolling: Effect of grooved rolling die geometry on texture uniformity. *Int. J. Refract. Met. Hard Mater.* **2017**, *66*, 44–51. [CrossRef]
- 34. Kalidindi, S.R.; Duvvuru, H.K.; Knezevic, M. Spectral calibration of crystal plasticity models. *Acta Mater.* **2006**, *54*, 1795–1804. [CrossRef]
- 35. Jahedi, M.; Knezevic, M.; Paydar, M. High-pressure double torsion as a severe plastic deformation process: Experimental procedure and finite element modeling. *J. Mater. Eng. Perform.* **2015**, 24, 1471–1482. [CrossRef]
- 36. Jahedi, M.; Beyerlein, I.J.; Paydar, M.H.; Knezevic, M. Effect of grain shape on texture formation during severe plastic deformation of pure copper. *Adv. Eng. Mater.* **2018**, *20*, 1600829.
- 37. Jahedi, M.; Beyerlein, I.J.; Paydar, M.H.; Zheng, S.; Xiong, T.; Knezevic, M. Effects of pressure and number of turns on microstructural homogeneity developed in high-pressure double torsion. *Metall. Mater. Trans. A* **2017**, *48*, 1249–1263. [CrossRef]
- 38. Jahedi, M.; Paydar, M.H.; Knezevic, M. Enhanced microstructural homogeneity in metal-matrix composites developed under high-pressure-double-torsion. *Mater. Charact.* **2015**, *104*, 92–100. [CrossRef]
- 39. Jahedi, M.; Paydar, M.H.; Zheng, S.; Beyerlein, I.J.; Knezevic, M. Texture evolution and enhanced grain refinement under high-pressure-double-torsion. *Mater. Sci. Eng. A* **2014**, *611*, 29–36. [CrossRef]
- 40. Qiao, X.G.; Gao, N.; Starink, M.J. A model of grain refinement and strengthening of al alloys due to cold severe plastic deformation. *Philos. Mag.* **2012**, 92, 446–470. [CrossRef]
- 41. Bachmaier, A.; Pippan, R. Generation of metallic nanocomposites by severe plastic deformation. *Int. Mater. Rev.* **2013**, *58*, 41–62. [CrossRef]
- 42. Xu, C.; Xia, K.; Langdon, T.G. The role of back pressure in the processing of pure aluminum by equal-channel angular pressing. *Acta Mater.* **2007**, *55*, 2351–2360. [CrossRef]
- 43. Harsha, R.; Kulkarni, V.M.; Babu, B.S. Severe plastic deformation-a review. Mater. Today Proc. 2018, 5, 22340–22349. [CrossRef]
- 44. Valiev, R.; Korznikov, A.; Mulyukov, R. Structure and properties of ultrafine-grained materials produced by severe plastic deformation. *Mater. Sci. Eng. A* 1993, 168, 141–148. [CrossRef]
- 45. Sadasivan, N.; Balasubramanian, M. Severe plastic deformation of tubular materials–process methodology and its influence on mechanical properties–a review. *Mater. Today Proc.* **2021**. [CrossRef]
- 46. Zare, H.; Jahedi, M.; Toroghinejad, M.R.; Meratian, M.; Knezevic, M. Microstructure and mechanical properties of carbon nanotubes reinforced aluminum matrix composites synthesized via equal-channel angular pressing. *Mater. Sci. Eng. A* **2016**, 670, 205–216. [CrossRef]
- 47. Zare, H.; Jahedi, M.; Toroghinejad, M.R.; Meratian, M.; Knezevic, M. Compressive, shear, and fracture behavior of cnt reinforced al matrix composites manufactured by severe plastic deformation. *Mater. Des.* **2016**, *106*, 112–119. [CrossRef]
- 48. Chen, X.; Huang, G.; Liu, S.; Han, T.; Jiang, B.; Tang, A.; PAN, F.; ZHU, Y. Grain refinement and mechanical properties of pure aluminum processed by accumulative extrusion bonding. *Trans. Nonferrous Met. Soc. China* **2019**, 29, 437–447. [CrossRef]
- 49. Chen, X.; Xia, D.; Zhang, J.; Huang, G.; Liu, K.; Tang, A.; Jiang, B.; Pan, F. Ultrafine-grained al–zn–mg–cu alloy processed via cross accumulative extrusion bonding and subsequent aging: Microstructure and mechanical properties. *J. Alloys Compd.* **2020**, 846, 156306. [CrossRef]
- Chen, X.; Zhang, J.; Xia, D.; Huang, G.; Liu, K.; Jiang, B.; Tang, A.; Pan, F. Microstructure and mechanical properties of 1060/7050 laminated composite produced via cross accumulative extrusion bonding and subsequent aging. J. Alloys Compd. 2020, 826, 154094. [CrossRef]

Metals **2021**, 11, 389 25 of 25

51. Liu, S.; Zhang, J.; Chen, X.; Huang, G.; Xia, D.; Tang, A.; Zhu, Y.; Jiang, B.; Pan, F. Improving mechanical properties of heterogeneous mg-gd alloy laminate via accumulated extrusion bonding. *Mater. Sci. Eng. A* **2020**, 785, 139324. [CrossRef]

- 52. Mehr, V.Y.; Toroghinejad, M.R.; Rezaeian, A. The effects of oxide film and annealing treatment on the bond strength of al–cu strips in cold roll bonding process. *Mater. Des.* **2014**, 53, 174–181. [CrossRef]
- 53. Ana, S.A.; Reihanian, M.; Lotfi, B. Accumulative roll bonding (arb) of the composite coated strips to fabricate multi-component al-based metal matrix composites. *Mater. Sci. Eng. A* **2015**, *647*, 303–312. [CrossRef]
- 54. Mozaffari, A.; Hosseini, M.; Manesh, H.D. Al/ni metal intermetallic composite produced by accumulative roll bonding and reaction annealing. *J. Alloys Compd.* **2011**, *509*, 9938–9945. [CrossRef]
- 55. Jamaati, R.; Toroghinejad, M.R. Effect of friction, annealing conditions and hardness on the bond strength of al/al strips produced by cold roll bonding process. *Mater. Des.* **2010**, *31*, 4508–4513. [CrossRef]
- 56. Chitkara, N.; Aleem, A. Extrusion of axi-symmetric bi-metallic tubes from solid circular billets: Application of a generalised upper bound analysis and some experiments. *Int. J. Mech. Sci.* **2001**, *43*, 2833–2856. [CrossRef]
- 57. Chaudhari, G.; Andhale, S.; Patil, N. Experimental evaluation of effect of die angle on hardness and surface finish of cold forward extrusion of aluminum. *Int. J. Emerg. Technol. Adv. Eng.* **2012**, *2*, 334–338.
- 58. Vaidyanath, L.; Nicholas, M.; Milner, D. Pressure welding by rolling. Br. Weld. J. 1959, 6, 13–28.
- 59. Hua, F.; Yang, Y.; Zhang, Y.; Guo, M.; Guo, D.; Tong, W.; Hu, Z. Three-dimensional finite element analysis of tube spinning. *J. Mater. Process. Technol.* **2005**, *168*, 68–74. [CrossRef]
- 60. Xia, Q.; Xie, S.W.; Huo, Y.; Ruan, F. Numerical simulation and experimental research on the multi-pass neck-spinning of non-axisymmetric offset tube. *J. Mater. Process. Technol.* **2008**, 206, 500–508. [CrossRef]
- 61. Ardeljan, M.; Knezevic, M.; Nizolek, T.; Beyerlein, I.J.; Mara, N.A.; Pollock, T.M. A study of microstructure-driven strain localizations in two-phase polycrystalline hcp/bcc composites using a multi-scale model. *Int. J. Plast.* **2015**, 74, 35–57. [CrossRef]
- 62. Dallas, D.B. Tool and Manufacturing Engineers Handbook, 3rd ed.; McGraw Hill Inc.: New York, NY, USA, 1976.
- 63. McCauley, E.O.A.C.J. Tool Steels, 28th ed.; Industrial Press Inc.: New York, NY, USA, 2008.
- 64. Thermal Diffusion (VCTDH) Coatings. Available online: https://www.ibccoatings.com/thermal-diffusion-td-coatings (accessed on 12 January 2021).
- 65. de Moraes Costa, A.L.; da Silva, U.S.; Valberg, H.S. On the friction conditions in fem simulations of cold extrusion. *Procedia Manuf.* **2020**, *47*, 231–236. [CrossRef]
- 66. Zecevic, M.; McCabe, R.J.; Knezevic, M. A new implementation of the spectral crystal plasticity framework in implicit finite elements. *Mech. Mater.* **2015**, *84*, 114–126. [CrossRef]
- 67. Knezevic, M.; Beyerlein, I.J. Multiscale modeling of microstructure-property relationships of polycrystalline metals during thermo-mechanical deformation. *Adv. Eng. Mater.* **2018**, 20, 1700956. [CrossRef]
- 68. Knezevic, M.; Kalidindi, S.R. Crystal plasticity modeling of microstructure evolution and mechanical fields during processing of metals using spectral databases. *JOM* **2017**, *69*, 830–838. [CrossRef]
- 69. Madaah-Hosseini, H.; Kokabi, A. Cold roll bonding of 5754-aluminum strips. Mater. Sci. Eng. A 2002, 335, 186–190. [CrossRef]
- 70. Fattah-Alhosseini, A.; Imantalab, O.; Mazaheri, Y.; Keshavarz, M. Microstructural evolution, mechanical properties, and strain hardening behavior of ultrafine grained commercial pure copper during the accumulative roll bonding process. *Mater. Sci. Eng. A* **2016**, *650*, 8–14. [CrossRef]
- 71. Babaei, A.; Mashhadi, M. Tubular pure copper grain refining by tube cyclic extrusion–compression (tcec) as a severe plastic deformation technique. *Prog. Nat. Sci. Mater. Int.* **2014**, 24, 623–630. [CrossRef]
- 72. Alvandi, H.; Farmanesh, K. Microstructural and mechanical properties of nano/ultra-fine structured 7075 aluminum alloy by accumulative roll-bonding process. *Procedia Mater. Sci.* 2015, 11, 17–23. [CrossRef]